

On Evaluating Adversarial Robustness of Volumetric Medical Segmentation Models

Hashmat Shadab Malik¹
hashmat.malik@mbzuai.ac.ae

Numan Saeed¹
numan.saeed@mbzuai.ac.ae

Asif Hanif¹
asif.hanif@mbzuai.ac.ae

Muzammal Naseer^{1,2}
muzammal.naseer@mbzuai.ac.ae

Mohammad Yaqub¹
mohammad.yaqub@mbzuai.ac.ae

Salman Khan^{1,2}
salman.khan@mbzuai.ac.ae

Fahad Shahbaz Khan^{1,3}
fahad.khan@mbzuai.ac.ae

¹ Mohamed bin Zayed University of AI

² Australian National University

³ Linköping University

Abstract

Volumetric medical segmentation models have achieved significant success on organ and tumor-based segmentation tasks in recent years. However, their vulnerability to adversarial attacks remains largely unexplored, raising serious concerns regarding the real-world deployment of tools employing such models in the healthcare sector. This underscores the importance of investigating the robustness of existing models. In this context, our work aims to empirically examine the adversarial robustness across current volumetric segmentation architectures, encompassing Convolutional, Transformer, and Mamba-based models. We extend this investigation across four volumetric segmentation datasets, evaluating robustness under both *white box* and *black box* adversarial attacks. Overall, we observe that while both pixel and frequency-based attacks perform reasonably well under *white box* setting, the latter performs significantly better under transfer-based *black box* attacks. Across our experiments, we observe transformer-based models show higher robustness than convolution-based models with Mamba-based models being the most vulnerable. Additionally, we show that large-scale training of volumetric segmentation models improves the model's robustness against adversarial attacks. The code and pretrained models will be made available on [Github](#).

1 Introduction

The field of computer vision has witnessed remarkable progress in recent years, leading to substantial improvements across a diverse range of vision-based tasks spanning various domains. Despite this advancement, deep learning models are widely known to be susceptible

to *adversarial attacks* [0, 11, 15, 55, 46, 48], which involves introducing carefully crafted, imperceptible perturbations to images, leading to incorrect response from the model. Based on the amount of information available about the target model, adversarial attacks can be broadly classified into *white-box* attacks, where the attacker has complete information and can directly craft an attack on the target model, and the more practical setting of *black-box* attacks, where access to the model is limited, and adversarial examples are crafted using query-based [6, 10, 59] and transfer-based approaches [13, 57, 40]. Understanding the vulnerabilities of models against these attacks is crucial for deploying them in security-critical applications such as healthcare systems, as it offers insights into identifying blind spots in the models to ensure their robustness and reliability.

Several works [8, 9, 41, 42, 44] have extensively investigated the adversarial robustness of Convolutional Neural Networks (CNNs) [22, 45] and Vision Transformers (ViTs) [14, 49]. However, these investigations have predominantly focused on models trained with natural images for the task of image classification, emphasizing the need to assess the robustness of vision-based models in the medical domain to ensure their safe deployment in healthcare systems. Within the medical domain, volumetric image segmentation stands out as an essential task for diagnoses, enabling the identification and delineation of organs or tumors within three-dimensional medical images such as Computed Tomography (CT) or Magnetic Resonance Imaging (MRI) scans [0, 6, 27, 53]. While in recent years, the performance of volumetric segmentation models has improved significantly [23], there has been limited works studying and evaluating the susceptibility of these models to adversarial attacks [12, 19]. To address this gap, our study aims to establish the first comprehensive benchmark for evaluating the robustness of volumetric segmentation models against adversarial attacks.

For thoroughly evaluating the robustness of current volumetric segmentation models, we consider a wide range of architectures, encompassing Convolutional, Transformer, and the recently introduced Mamba-based models [54]. We expand the scope of our analysis by evaluating these segmentation models across four diverse 3D segmentation datasets consisting of CT and MRI scans. We first evaluate the performance of these architectures under *white-box* setting against different pixel and frequency-based attacks expanding on previous works which have done limited analysis under this setting [12, 19]. Further, we evaluate the models against transfer-based *black-box* attacks by transferring the adversarial examples crafted on the surrogate model to unseen target models. To the best of our knowledge, no existing work has investigated the transferability of adversarial examples among different volumetric medical segmentation models, a practical setting that can be encountered in real-world scenarios. Furthermore, we expand our analysis by evaluating the current vision foundation model [51] on transfer-based attacks to assess its robustness capabilities, given its training on large-scale 3D medical datasets. Our contributions are as follows:

- We provide the first comprehensive benchmark for analyzing the robustness of Convolution, Transformer, and Mamba-based volumetric medical image segmentation models against adversarial attacks.
- While all models show vulnerability to pixel and frequency-based attacks under *white-box* setting, the latter shows significant transferability across models in the *black-box* setting. Furthermore, transformer-based models in general exhibit higher robustness against adversarial attacks, while Mamba-based models are more vulnerable.
- Vision foundational models trained on large-scale datasets exhibit better robustness against *black-box* attacks.

2 Background and Related Work

Notations and Terminologies. A clean volumetric image is represented as $x \in \mathbb{R}^{H \times W \times D}$, with its binary segmentation mask $y \in \{0, 1\}^{C \times H \times W \times D}$, where C signifies the number of classes. A volumetric segmentation model \mathcal{F} , predicts the segmentation mask of the input images, expressed as $\mathcal{F} : \mathcal{X} \mapsto \mathcal{Y}$, where \mathcal{X} and \mathcal{Y} denote the sets of input images and corresponding segmentation masks, respectively. An adversarial attack crafted on model \mathcal{F} involves manipulating the input image x , typically in the pixel or frequency domains to generate the adversarial image x' . The adversarial manipulation $\delta = (x' - x)$ while imperceptible, leads to an incorrect response from the model $\mathcal{F}(x') \neq \mathcal{F}(x)$.

Adversarial Attacks. The vulnerability of deep learning models to adversarial examples [15, 26, 48] has prompted the research community to investigate the robustness of current models against various forms of adversarial attacks [0, 11, 15, 55, 46]. Several works have delved into analyzing and comparing the adversarial robustness of CNN and transformer-based classifier models trained on natural images [9, 9, 41, 42, 44]. A few works in the natural domain have focused on designing adversarial attacks tailored for 2D segmentation models [0, 18, 24]. These methods propose a dynamic pixel-level loss, enabling the attack to direct attention to regions of the image where the model maintains accurate predictions during the attack iterations. Focusing on the task of volumetric medical segmentation, limited works [2, 19] have delved into understanding the robustness of medical segmentation models. In [2], adversarial attacks proposed for classification tasks are extended to target volumetric medical segmentation models, while [19] proposes a frequency domain attack to fool the medical segmentation models by dropping imperceptible information in the frequency domain of the input image. However, both works provide a limited examination of robustness, confining the scope to just *white-box* attacks across a restricted range of models and datasets. In contrast, our work aims to provide a comprehensive empirical evaluation of current volumetric medical segmentation architectures across adversarial attacks encompassing both *white-box* and *black-box* settings.

Volumetric Medical Segmentation Models. Convolutional Neural Networks (CNNs) and Transformers are two popular architectures used in volumetric medical image segmentation. CNNs, such as U-Net [43] and SegResNet [58], are particularly good at extracting hierarchical image features. The shared weights in CNN-based models across the features help to capture local-level information, making them well-suited for capturing translational invariances. In contrast to CNNs, transformer-based models [14, 51] attention mechanism captures global information, increasing the effective receptive field of the model [52]. To exploit the complementary strengths of both, hybrid-based models like TransUNet [9], UNETR [21], and SwinUNETR [20] have been proposed to incorporate both CNNs and Transformers into the network. While Transformer models excel at modeling long-range dependencies via their attention mechanism, a significant drawback is their quadratic computational scaling with input size, making them resource-intensive for 3D medical segmentation. Recently, state space sequence models (SSMs) [16, 17] proposed in the natural language domain have been adapted for vision tasks [8, 29, 30, 52], providing the capability to handle long-range dependencies while maintaining a linear computational cost. In the medical segmentation domain, [54] introduced UMamba, a network merging CNNs' local feature extraction with SSMs' efficient long-range dependency handling capabilities. Based on the above model architectures, our work provides an empirical robustness evaluation of CNNs, transformers, and recently introduced state space models against adversarial attacks in the context of volumetric medical segmentation. Furthermore, given the recent trend of enhancing the

generalization capabilities of vision models through large-scale training, we extend our analysis to examine the robustness of SAM-Med3D [50], a foundational model for volumetric segmentation trained on large-scale segmentation datasets.

3 Research Scope

Research Goal. In recent years, volumetric medical segmentation models have achieved significant success on organ and tumor-based segmentation tasks. However, the vulnerability of these models to adversarial attacks raises serious concerns about their real-world deployment in the healthcare sector. This vulnerability raises doubts among clinicians regarding the reliability of tools employing such models and underscores the importance of investigating and enhancing their robustness. In this context, our work aims to *empirically* investigate the adversarial robustness across different volumetric segmentation architectures, encompassing Convolutional, Transformer, and Mamba-based models. We extend this investigation across four volumetric segmentation datasets, assessing the models’ robustness under both *white-box* and *black-box* adversarial attack scenarios. Our work does not claim to provide theoretical reasoning behind the robustness behavior across models, instead as one of the first works in studying the vulnerability of volumetric segmentation models, we provide detailed empirical evaluations across different adversarial settings. Furthermore, we conduct frequency-based analyses to gain further insights into the models’ behavior to adversarial attacks and examine the impact of large-scale training on the model’s robustness. While the scope of this work is limited, we hope this work paves the way for future research focusing on the robustness of medical segmentation models.

Datasets. We utilize four 3D segmentation datasets: BTCV (30 *abdominal CT scans from liver cancer patients with 13 organ annotations*) [22], ACDC (150 *MRI images of cardiac abnormalities with heart organ annotations*) [6], HeCtor (524 *CT/PET scans of head and neck cancer patients annotated for primary and nodal tumor*) [4], and AbdomenCT-1k (1112 *abdominal CT scans from diverse medical centers with annotations for abdominal region*) [43]. For more details about the datasets, refer to Appendix A.

Models. In our experiments, we consider CNN models (UNet [44] and SegResNet [68]), Transformer models (UNETR [24] and Swin-UNETR [20]), and recently introduced Visual State Space models (UMamba-B and UMamba-E [64]). All models are trained from scratch on the four mentioned datasets with the input size of $96 \times 96 \times 96$, following the training methodology outlined in [49]. Further, we consider SAM-Med3D [50], a vision foundation model for volumetric medical images trained on large-scale segmentation datasets.

Adversarial Attacks and Metrics. We consider two categories of adversarial attacks: pixel-based attacks, which include Fast Gradient Sign Method (FGSM) [45], Projected Gradient Descent (PGD) [65], and Cosine-PGD (CosPGD) [40], and frequency-based attacks, for which we consider Volumetric Adversarial Frequency Attack (VAFA) [49]. CosPGD, originally proposed for 2D segmentation tasks, is adapted to work in 3D segmentation scenarios, whereas VAFA operates directly on volumetric data. All the above methods are based on minimizing the Dice Similarity Score (DSC) [47] during the attack optimization. We also report model performance on additive Gaussian Noise (GN). For evaluating segmentation task, we report the Dice Similarity Coefficient (DSC) and the mean 95% Hausdorff Distance (HD95) score on clean samples. To assess the Attack Success Rate (ASR), we introduce two metrics, ASR-D and ASR-H, which measure the average performance decline of models

Dataset	Attack	UNet		SegResNet		UNETR		SwinUNETR		UMamba-B		UMamba-E		Average	
		ASR-D	ASR-H	ASR-D	ASR-H	ASR-D	ASR-H	ASR-D	ASR-H	ASR-D	ASR-H	ASR-D	ASR-H	ASR-D	ASR-H
BTCV	Clean	75.72	9.15	80.84	8.14	72.53	15.08	78.07	10.01	78.37	8.12	77.06	11.11	-	-
	GN	0.32	1.16	0.50	0.30	0.20	-0.63	0.63	-0.28	0.68	1.32	1.72	10.69	0.675	2.093
	FGSM	26.23	39.08	20.87	29.22	21.55	29.78	19.27	30.84	19.74	27.33	23.47	34.43	21.86	31.78
	PGD	43.66	80.30	60.73	91.99	24.52	38.70	23.08	54.42	48.29	89.92	47.55	93.40	41.31	74.79
	CosPGD	43.21	66.74	61.16	18.60	25.07	36.06	25.14	48.45	47.41	74.63	45.96	68.58	41.33	52.18
	VAFa	56.23	77.60	58.84	64.02	45.85	43.75	53.77	52.37	61.72	70.92	60.61	80.24	56.17	64.82
ACDC	Clean	85.52	5.75	89.65	2.56	76.37	16.31	84.19	7.93	88.22	6.01	80.91	8.48	-	-
	GN	0.51	-0.08	0.39	0.33	1.49	2.18	1.13	2.76	1.27	0.67	2.80	3.19	1.265	1.508
	FGSM	29.97	16.24	23.07	9.32	43.21	13.46	28.08	13.90	15.67	15.18	29.26	15.74	28.21	13.97
	PGD	64.10	33.39	69.23	34.78	54.06	19.13	62.50	29.06	63.27	28.65	55.90	23.95	61.51	28.16
	CosPGD	62.90	31.09	67.32	36.05	53.29	18.49	61.69	28.27	62.68	25.31	56.47	23.07	60.73	27.05
	VAFa	35.67	21.69	35.18	20.82	26.98	6.32	35.75	17.64	34.84	19.21	29.30	17.24	32.95	17.15
Hecktor	Clean	73.91	11.36	74.73	11.08	72.36	14.61	71.61	22.07	73.49	10.89	72.19	13.29	-	-
	GN	1.80	1.61	1.76	-0.87	1.09	0.25	1.97	2.70	1.57	1.24	5.63	-0.42	2.303	0.751
	FGSM	30.13	26.43	27.03	21.16	27.47	20.47	27.79	30.88	23.33	19.23	25.04	18.36	26.80	22.76
	PGD	39.84	67.25	41.71	70.09	37.43	59.97	37.49	56.78	39.18	67.50	37.90	64.96	38.93	64.43
	CosPGD	39.69	67.26	41.32	70.20	37.47	59.23	37.40	55.55	39.08	67.55	37.82	64.56	38.80	64.06
	VAFa	29.61	30.83	27.18	22.00	24.35	19.21	27.17	20.07	24.22	25.10	27.38	23.55	26.65	23.46
Abdomen-CT	Clean	76.79	19.72	80.89	13.30	71.35	27.73	79.33	25.79	81.08	15.51	78.05	18.31	-	-
	GN	0.66	2.25	3.30	4.86	0.22	6.64	0.38	3.30	1.75	1.21	1.78	-0.15	1.348	3.018
	FGSM	29.94	40.47	30.16	35.77	22.87	31.12	25.87	45.24	29.72	38.38	29.24	33.82	27.97	37.47
	PGD	47.65	71.13	63.47	93.43	26.52	48.35	32.38	63.09	62.88	96.28	54.46	78.53	47.89	75.14
	CosPGD	45.99	57.75	62.01	88.95	26.71	46.61	32.54	57.13	62.09	86.38	53.06	63.70	47.07	66.75
	VAFa	55.87	68.47	63.21	71.61	49.01	60.35	53.90	50.62	66.09	76.58	64.17	74.60	58.71	67.04
Average	-	42.54	49.73	47.03	48.63	34.15	34.44	36.49	40.89	43.76	51.76	42.35	48.67	-	-

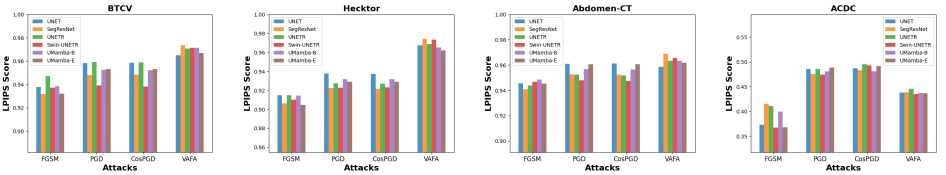
Table 1: Performance of models against *white box* attacks across different datasets is reported.

Figure 1: LPIPS scores for adversarial examples crafted on different segmentation models.

under adversarial attacks:

$$\text{ASR-D} = \frac{1}{|\mathcal{D}_{\text{test}}|} \sum_{x,y \in \mathcal{D}_{\text{test}}} \left| \text{DSC}(\mathcal{F}(x), y) - \text{DSC}(\mathcal{F}(x'), y) \right| \quad (1)$$

$$\text{ASR-H} = \frac{1}{|\mathcal{D}_{\text{test}}|} \sum_{x,y \in \mathcal{D}_{\text{test}}} \left| \text{HD95}(\mathcal{F}(x'), y) - \text{HD95}(\mathcal{F}(x), y) \right| \quad (2)$$

4 Experimental Results

4.1 Robustness against White-Box Attacks

In this section, we examine the robustness of segmentation models in white-box settings. For pixel-based attacks, we consider FGSM [48], PGD [85] and CosPGD [40] and use perturbation budget $\epsilon = \frac{8}{255}$ and set 20 optimization steps for iterative attacks. For frequency-based attack VAFa [49], we generate adversarial examples with $q_{\max} = 30$, employing a patch size of $32 \times 32 \times 32$, while keeping other parameters consistent with the default settings as outlined in [49]. Adversarial examples are generated on the validation sets of BTCV, ACDC, Hecktor, and Abdomen-CT datasets by attacking the models trained on the respective datasets. In Table 1, we show segmentation model performance based on attack success rates for DSC and HD95 metrics. We observe that for the BTCV and Abdomen-CT datasets, which are utilized for the organ segmentation task, VAFa achieves the highest ASR-D among all attacks. On average, across all the models, VAFa demonstrates an increase of 14.84%

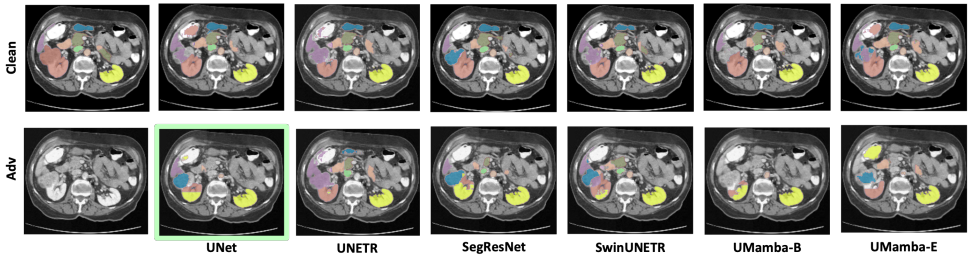


Figure 2: Comparing multi-organ segmentation across various models under transfer-based *black box* attacks, where adversarial examples are generated on UNet and transferred to other unseen models.

and 11.64% over the best pixel-based attacks for the BTCV and Abdomen-CT datasets, respectively. However, for ACDC and HeCktoR datasets, which are used for MRI-based organ segmentation and CT-based tumor segmentation, we observe iterative pixel-based attacks perform much better than other attacks, especially for the ACDC dataset (an increase of 28.56% over VAFA). When examining the average attack success rate across all datasets, we note that CNN-based models exhibit the least robustness, with SegResNet having the highest average ASR-D of 47.03%. Following closely are UNet and UMamba-base models. In contrast, transformer-based models demonstrate the highest level of robustness, with UNETR exhibiting an average ASR-D of 34.15%.

We further look into the perceptual quality of adversarial images crafted of different models across different datasets. In Figure 1, we report LPIPs score [50] to compute the similarity between the adversarial and clean volumetric image. Our results reveal a general trend: pixel-based attacks tend to reduce the LPIPS score more than the frequency-based VAFA attack. Specifically, the single-step FGSM attack demonstrates the most significant decrease in score. Notably, VAFA achieves higher similarity scores with respect to the clean images, suggesting the potential for generating even stronger adversarial examples by increasing the bound q_{max} while maintaining a comparable LPIPS score compared to other attacks. However, this trend deviates on the ACDC dataset, where all attacks lead to a notable drop in the LPIPS score. Iterative pixel-based attacks yield the highest LPIPS score, followed by VAFA and FGSM attacks. Further analyses on *white-box* attacks with perturbation budgets: $\epsilon = \frac{4}{255}$ for pixel-based attacks and $q_{max} \in \{10, 20\}$ in Appendix C.

4.2 Robustness against Black-Box Attacks

In this section, we evaluate and compare the robustness of different models against transfer-based *black-box* attacks. These attacks exploit the *transferability* property of adversarial examples i.e., adversarial examples crafted on a surrogate model transfer to unknown target models. For our evaluation, we evaluate the transferability of all segmentation models by using them interchangeably as both surrogate and target models. In Table 2, 3, 4 and 5 we report results on transferability of models on BTCV, Abdomen-CT, ACDC, and HeCktoR dataset. On all the datasets except HeCktoR, we observe that frequency-based attacks demonstrate significant transferability across all models compared to pixel-based attacks. Additionally, among pixel-based attacks, the single-step FGSM attack performs better, suggesting that adversarial examples crafted by iterative pixel-based attacks tend to overfit on the surrogate models, resulting in lower transferability[13]. This is evident as pixel-based iterative attacks outperform the FGSM attack on the surrogate model. While one-step gradient methods do not overfit on the surrogate model[25], they tend to have a low success rate, making them

Target → Surrogate ↓	Attack	UNet		SegResNet		UNETR		SwinUNETR		UMamba-B		UMamba-E		Average	
		ASR-D	ASR-H	ASR-D	ASR-H	ASR-D	ASR-H	ASR-D	ASR-H	ASR-D	ASR-H	ASR-D	ASR-H	ASR-D	ASR-H
	Clean	75.72	9.15	80.84	8.14	72.53	15.08	78.07	10.01	78.37	8.12	77.06	11.11	-	-
	GN	0.32	1.16	0.50	0.30	0.20	-0.63	0.63	-0.28	0.68	1.32	1.72	10.69	0.675	2.050
UNet	FGSM	26.23	39.08	2.86	1.35	2.02	0.91	3.10	2.25	3.73	1.91	5.22	14.84	3.386	4.640
	PGD	43.66	80.30	1.06	0.59	0.51	0.20	1.18	0.68	1.45	0.90	2.32	2.75	1.304	1.020
	CosPGD	43.21	66.74	1.06	0.57	0.54	-0.14	1.20	1.01	1.54	2.24	2.27	5.39	1.322	1.810
	VAFa	56.23	77.60	46.45	45.17	27.04	19.60	36.59	26.99	49.37	49.13	57.68	60.84	43.42	40.35
SegResNet	FGSM	4.02	2.86	20.87	29.22	2.60	0.26	5.59	1.80	9.64	6.65	9.11	11.63	6.192	4.640
	PGD	2.38	4.79	60.73	91.99	1.79	0.07	3.12	2.28	7.58	6.13	6.98	10.56	4.370	4.766
	CosPGD	2.43	4.61	61.16	88.60	1.78	0.04	3.03	1.74	7.87	6.04	7.27	10.20	4.476	4.526
	VAFa	39.29	35.28	58.84	64.02	22.37	13.11	32.53	26.82	49.98	47.75	57.53	58.34	40.34	36.26
UNETR	FGSM	4.83	2.92	4.71	2.37	21.55	29.78	6.59	2.96	5.90	2.23	5.85	3.94	5.576	2.884
	PGD	3.48	4.34	2.38	1.43	24.52	38.70	3.43	2.61	3.75	2.17	4.33	4.18	3.474	2.946
	CosPGD	3.41	4.46	2.11	1.15	25.07	36.06	3.24	3.43	3.59	1.68	4.25	4.32	3.320	3.008
	VAFa	35.45	26.09	38.29	26.70	45.85	43.75	36.17	29.53	42.21	35.85	45.59	34.34	39.54	30.50
SwinUNETR	FGSM	4.25	3.43	5.75	2.72	3.59	0.66	19.27	30.83	6.49	3.34	6.91	8.01	5.398	3.632
	PGD	3.44	4.53	2.92	1.47	2.36	2.09	23.98	54.42	3.75	3.44	4.87	9.59	3.468	4.224
	CosPGD	3.32	5.44	2.97	1.57	2.33	3.05	25.14	48.45	3.65	3.91	4.87	10.01	3.428	4.796
	VAFa	46.50	44.96	50.54	36.06	33.84	23.14	53.77	52.37	52.68	41.47	55.10	45.35	47.73	38.20
UMamba-B	FGSM	4.33	4.99	8.88	5.15	2.40	0.89	5.44	2.72	19.74	27.33	11.31	12.02	6.472	5.154
	PGD	2.45	2.87	4.73	4.45	1.47	0.53	2.48	2.30	48.29	89.92	9.34	12.52	4.094	4.534
	CosPGD	2.42	3.77	4.43	4.64	1.42	-0.11	2.33	1.71	47.41	74.63	8.80	14.33	3.880	4.868
	VAFa	40.54	33.63	50.39	41.58	25.60	31.34	35.18	28.18	61.72	70.62	60.05	62.62	42.35	37.04
UMamba-E	FGSM	3.13	3.18	5.15	3.18	2.04	1.19	3.59	1.01	7.01	6.46	23.47	34.43	4.184	3.004
	PGD	1.33	4.51	1.75	1.41	0.84	-0.04	1.16	1.22	2.79	2.62	47.55	93.40	1.574	1.944
	CosPGD	1.31	4.58	1.70	1.80	0.78	0.30	1.12	1.23	2.54	3.40	45.96	68.58	1.490	2.262
	VAFa	31.64	27.63	38.37	28.60	18.92	10.49	23.66	15.98	45.47	39.01	60.61	80.24	31.61	24.34

Table 2: Performance of models against transfer-based *black box* attacks on BTCV dataset.

Target → Surrogate ↓	Attack	UNet		SegResNet		UNETR		SwinUNETR		UMamba-B		UMamba-E		Average	
		ASR-D	ASR-H	ASR-D	ASR-H	ASR-D	ASR-H	ASR-D	ASR-H	ASR-D	ASR-H	ASR-D	ASR-H	ASR-D	ASR-H
	Clean	76.79	19.72	80.89	13.30	71.35	27.73	79.33	25.79	81.08	15.51	78.05	18.31	-	-
	GN	0.66	2.25	3.30	4.86	0.22	6.64	0.38	3.30	1.75	1.27	1.78	-0.15	1.348	3.028
UNet	FGSM	29.94	40.47	8.99	5.20	2.45	7.27	4.34	5.95	8.53	7.17	7.81	6.12	6.424	6.340
	PGD	47.65	71.13	4.54	2.26	1.16	5.19	1.60	2.98	3.86	3.78	3.58	1.84	2.948	3.210
	CosPGD	45.99	57.75	4.45	2.36	1.11	6.14	1.47	2.73	3.65	2.76	3.47	1.94	2.830	3.190
	VAFa	55.87	68.47	54.27	53.09	32.99	35.84	40.58	31.49	58.72	55.74	59.16	56.80	49.14	46.59
SegResNet	FGSM	6.29	3.87	30.16	35.77	2.64	6.93	5.04	2.17	16.17	13.63	14.11	8.41	8.850	7.002
	PGD	3.03	3.05	63.47	93.43	1.45	4.85	2.43	3.04	10.21	8.06	8.24	6.49	5.070	5.100
	CosPGD	2.72	4.35	62.01	88.95	1.42	4.53	2.33	3.38	9.49	7.62	7.69	5.250	4.730	5.030
	VAFa	38.32	31.64	63.21	71.61	28.02	26.86	34.33	22.06	58.65	48.33	58.30	46.32	43.52	35.04
UNETR	FGSM	6.41	3.83	9.21	3.36	22.87	31.12	7.79	5.69	9.38	9.68	8.77	3.11	8.312	5.134
	PGD	4.22	3.27	6.04	3.89	26.52	48.35	4.05	5.17	6.26	3.33	7.23	5.50	5.560	4.232
	CosPGD	4.12	3.01	5.78	3.75	26.71	46.61	3.87	4.82	6.26	2.96	7.05	4.74	5.416	3.856
	VAFa	37.11	28.88	48.26	42.75	49.01	60.35	41.22	28.70	51.48	38.72	51.28	40.31	45.87	35.87
SwinUNETR	FGSM	6.80	4.72	11.50	5.18	4.54	7.32	25.87	45.24	10.87	7.94	9.93	5.54	8.728	6.140
	PGD	4.12	4.42	7.70	4.90	2.58	10.62	32.38	63.09	6.69	7.92	6.65	5.92	5.548	6.760
	CosPGD	3.91	3.95	7.30	5.04	2.50	10.36	32.54	57.13	6.49	6.79	6.38	5.60	5.322	6.350
	VAFa	46.32	40.91	53.38	47.21	38.25	36.63	53.90	50.62	56.97	50.12	55.99	47.08	50.18	44.39
UMamba-B	FGSM	6.19	5.19	15.83	10.68	2.66	8.21	5.08	5.61	29.72	38.38	15.86	11.70	9.124	8.278
	PGD	3.30	2.45	11.14	8.54	1.42	4.98	2.44	2.64	62.88	96.28	12.33	10.23	6.130	5.770
	CosPGD	3.33	3.27	10.54	7.64	1.41	5.35	2.41	2.90	62.09	86.38	11.69	11.73	5.880	6.180
	VAFa	38.30	35.75	56.69	52.14	27.55	30.64	34.72	26.39	66.09	76.58	59.59	51.33	43.37	39.25
UMamba-E	FGSM	5.86	3.76	12.62	7.57	2.66	7.34	4.48	3.73	15.42	14.84	29.24	33.82	8.208	7.448
	PGD	2.59	1.99	7.07	4.28	1.10	4.39	1.78	3.10	9.90	7.60	54.46	78.53	4.488	4.270
	CosPGD	2.38	1.44	6.74	3.76	1.05	4.83	1.68	2.99	9.22	7.39	53.06	63.70	4.214	4.080
	VAFa	37.38	33.43	53.50	47.84	28.03	30.90	32.80	25.18	57.77	57.00	64.17	74.60	41.90	38.87

Table 3: Performance of models against transfer-based *black box* attacks on Abdomen-CT dataset.

ineffective for *black box* attacks. Frequency-based attacks alleviate this trade-off between white-box attacks and transferability, providing a high level of success on *white box* attacks while also being highly transferable. However, we note a general lack of transferability among all attacks on the HeCkToR dataset (Table 5). Interestingly, compared to iterative pixel and frequency-based attacks, single-step FGSM attack demonstrate better performance across all the models.

Target → Surrogate ↓	Attack	UNet		SegResNet		UNETR		SwinUNETR		UMamba-B		UMamba-E		Average	
		ASR-D	ASR-H	ASR-D	ASR-H	ASR-D	ASR-H	ASR-D	ASR-H	ASR-D	ASR-H	ASR-D	ASR-H	ASR-D	ASR-H
	Clean	85.52	5.75	89.65	2.56	76.37	16.31	84.19	7.93	88.22	6.01	80.91	8.48	-	-
	GN	0.51	-0.08	0.39	0.33	1.49	2.18	1.13	2.76	1.27	0.67	2.80	3.19	1.265	1.508
UNet	FGSM	29.97	16.24	3.00	1.99	3.05	2.56	3.07	3.29	3.64	5.18	5.95	4.94	3.742	3.590
	PGD	64.10	33.39	1.60	2.65	1.70	2.65	1.62	2.66	1.90	4.07	3.09	2.34	1.982	2.870
	CosPGD	62.90	31.09	1.47	2.56	2.01	2.42	1.27	2.19	1.72	3.91	3.58	3.49	2.010	2.910
	VAFAs	35.67	21.69	15.50	15.61	20.28	5.46	25.47	15.02	27.95	18.45	27.23	17.50	23.29	14.41
SegResNet	FGSM	1.89	0.57	23.07	9.32	3.34	3.41	3.78	4.82	7.07	13.94	6.34	5.98	4.484	5.744
	PGD	1.14	0.59	69.23	34.78	1.78	1.31	1.92	1.91	2.50	4.47	4.52	2.86	2.370	2.230
	CosPGD	0.98	0.33	67.32	36.05	1.58	1.74	1.75	1.65	2.53	3.57	4.50	2.84	2.270	2.030
	VAFAs	33.69	21.47	35.18	20.82	21.41	5.29	27.19	16.27	28.98	18.26	27.79	16.90	27.81	15.64
UNETR	FGSM	5.37	7.03	6.32	3.92	43.21	13.46	8.40	8.81	10.74	19.92	8.03	6.45	7.772	9.226
	PGD	2.27	7.94	4.11	4.63	54.06	19.13	4.07	7.26	7.55	16.47	12.54	8.50	6.108	8.960
	CosPGD	2.54	7.73	3.57	4.53	53.29	18.49	4.07	7.48	6.85	15.10	10.39	9.03	5.484	8.774
	VAFAs	32.85	20.91	15.47	13.22	26.98	6.32	28.29	16.54	29.95	18.84	28.75	16.61	27.06	17.22
SwinUNETR	FGSM	2.41	1.86	8.31	2.55	4.46	1.84	28.08	13.90	7.53	9.60	6.19	3.26	5.780	3.822
	PGD	1.48	1.74	5.28	4.19	4.64	2.91	62.50	29.06	5.80	9.22	8.76	4.29	5.192	4.470
	CosPGD	1.60	2.00	5.27	4.69	4.46	3.93	61.69	28.27	4.88	13.97	10.42	4.75	5.326	5.870
	VAFAs	34.02	21.19	19.47	14.60	22.87	6.94	35.75	17.64	30.54	19.00	28.39	16.79	27.06	15.70
UMamba-B	FGSM	3.97	8.78	6.38	2.55	4.54	3.68	4.58	5.81	15.67	15.18	9.37	6.38	5.768	5.440
	PGD	2.70	7.06	7.16	3.62	4.23	2.82	4.24	4.40	63.27	28.65	11.25	6.81	5.920	4.940
	CosPGD	2.94	4.51	6.96	4.81	3.87	2.47	4.05	4.04	62.68	25.31	11.98	6.38	5.960	4.440
	VAFAs	34.06	21.60	18.29	15.23	22.19	6.51	27.05	5.46	34.84	19.21	29.08	17.79	26.13	13.32
UMamba-E	FGSM	3.08	7.66	4.69	2.19	5.14	4.28	2.37	4.23	6.25	9.76	29.26	15.74	4.306	5.624
	PGD	0.86	0.36	1.94	0.87	1.86	1.85	1.24	1.24	2.10	1.45	55.90	23.95	1.600	1.150
	CosPGD	0.73	0.57	2.34	1.28	1.51	1.27	1.18	1.59	2.03	1.13	56.47	23.07	1.558	1.170
	VAFAs	30.51	21.33	14.08	13.21	18.97	4.49	23.97	15.92	26.96	18.53	29.30	17.24	22.90	14.70

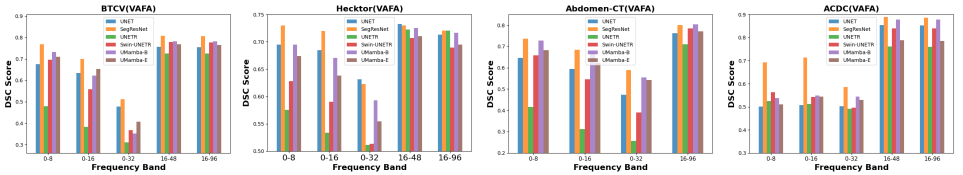
Table 4: Performance of models against transfer-based *black box* attacks on ACDC dataset.

To evaluate the effectiveness of surrogate models in crafting transferable adversarial examples, we report the average attack success rate across the target models. We observe that SwinUNETR surrogate models tend to craft the most transferable adversarial examples, achieving the highest average ASR-D of 47.73%, 50.18%, and 16.11% on BTCV, Abdomen-CT, and Hecktor datasets, respectively. However, on ACDC, it achieves a score of 27.06%, slightly lower than the 27.81% obtained by SegResNet. This effectiveness of SwinUNETR as a surrogate model can be attributed to its hybrid design, incorporating attributes of both CNN and transformer architectures, which contribute to the generalizability of adversarial examples across different architectures. Furthermore, upon averaging the ASR-D achieved by target models on the most transferable adversarial examples crafted by each surrogate model, we observe that the transformer-based model UNETR tend to be more robust. Similar to our *white box* analysis, UNETR achieves the lowest average ASR-D of 25.54%, 30.96%, 5.49% on BTCV, Abdomen-CT, and Hecktor, respectively. However, on ACDC, SegResNet with a score of 16.52% is more robust. Furthermore, consistent with Table 1, we note that Mamba-based models generally exhibit greater vulnerability to transfer-based attacks compared to their counterparts. In Figure 2, we show a qualitative comparison of transfer-based *black box* attack. Detailed analysis of *black box* setting is in Appendix F.

4.3 Frequency Analysis

Given the overall effectiveness of VAFAs in achieving higher transferability of adversarial examples compared to pixel-based attacks, in this section we delve deeper into the frequency analysis of VAFAs to study which frequency components lead to drop in performance of models. Following [44], we implement an adversarial attack incorporating a frequency filter M , restricting perturbations to specific frequency domains. The filter operation is defined as $x'_{\text{freq}} = \text{IDCT}(\text{DCT}(x' - x) \odot M) + x$, where DCT and IDCT denote Discrete Cosine Transform and its inverse, respectively. Similar to [44], using the filter M , we extract 3D cubes of vary-

Target → Surrogate ↓	Attack	UNet		SegResNet		UNETR		SwinUNETR		UMamba-B		UMamba-E		Average	
		ASR-D	ASR-H	ASR-D	ASR-H	ASR-D	ASR-H	ASR-D	ASR-H	ASR-D	ASR-H	ASR-D	ASR-H	ASR-D	ASR-H
	Clean	73.91	11.36	74.73	11.08	72.36	14.61	71.61	22.07	73.50	10.89	72.19	13.29	-	-
	GN	1.80	1.61	1.47	-1.00	1.08	-0.10	2.00	1.58	1.38	3.07	5.61	0.16	2.223	0.887
UNet	FGSM	30.13	26.43	15.62	7.15	5.87	2.62	12.85	8.54	14.24	7.74	14.72	5.79	12.66	6.370
	PGD	39.84	67.25	6.49	2.72	2.49	2.93	6.62	5.26	6.12	3.73	6.64	4.51	5.672	3.830
	CosPGD	39.69	67.26	5.25	1.84	2.34	2.22	5.50	3.93	4.92	2.22	5.98	2.81	4.798	2.600
	VAVA	29.61	30.83	5.92	3.72	9.26	3.76	6.51	-0.02	8.51	7.04	11.82	8.56	8.400	4.610
SegResNet	FGSM	13.29	10.07	27.03	21.16	4.85	2.56	14.60	8.13	19.58	16.23	17.06	7.79	13.87	8.956
	PGD	12.06	9.53	41.71	70.09	3.77	2.52	12.98	7.00	22.29	20.59	17.66	12.26	13.75	10.38
	CosPGD	11.92	8.53	41.32	70.20	3.55	2.02	12.87	7.12	23.25	21.36	18.04	9.99	13.93	9.800
	VAVA	4.84	6.41	27.18	22.00	6.12	3.10	6.06	-0.22	8.27	6.90	9.97	10.25	7.050	5.290
UNETR	FGSM	15.75	7.91	15.72	4.52	27.47	20.47	17.32	9.20	15.62	6.22	15.24	6.33	15.93	6.836
	PGD	15.58	8.99	13.71	5.81	37.43	59.97	16.06	10.68	13.12	8.51	13.21	4.560	14.33	7.710
	CosPGD	14.89	9.82	12.76	6.21	37.47	59.23	15.48	10.22	11.95	8.75	12.24	6.82	13.46	8.364
	VAVA	9.18	8.00	5.05	2.73	24.35	19.21	13.76	5.46	8.12	8.30	13.60	7.99	9.940	6.496
SwinUNETR	FGSM	15.95	10.46	19.14	7.89	7.70	4.78	27.79	30.88	18.96	13.82	18.80	8.19	16.11	9.028
	PGD	18.66	14.51	18.64	9.08	6.07	5.22	37.49	56.78	18.36	12.83	18.01	10.31	15.94	10.39
	CosPGD	18.08	12.52	18.12	10.27	5.83	4.82	37.40	55.55	18.13	14.29	17.49	9.79	15.53	10.34
	VAVA	8.33	8.40	6.35	4.38	10.39	5.64	27.17	20.07	7.57	5.64	13.63	7.39	9.250	6.290
UMamba-B	FGSM	13.57	7.27	19.23	7.70	5.13	2.12	15.32	10.95	23.34	19.23	17.68	6.57	14.18	6.922
	PGD	12.08	7.98	25.08	28.91	3.29	2.27	13.49	9.23	39.19	67.50	21.16	17.41	15.02	13.16
	CosPGD	12.04	8.98	26.16	29.73	3.24	3.00	12.56	8.95	39.09	67.55	20.80	18.87	14.96	13.71
	VAVA	7.30	9.50	9.74	5.24	8.25	3.89	7.08	-0.54	24.23	25.10	13.67	8.400	9.210	5.390
UMamba-E	FGSM	11.27	5.31	15.44	5.47	3.93	2.49	11.27	7.22	16.01	11.39	25.04	18.36	11.58	6.376
	PGD	4.61	3.59	5.96	1.14	1.77	0.92	4.69	3.07	6.75	5.84	37.90	64.96	4.756	2.910
	CosPGD	4.36	2.50	5.24	1.80	1.69	0.46	4.27	3.97	6.07	6.10	37.82	64.56	4.326	2.970
	VAVA	5.82	9.15	4.89	2.82	8.10	4.51	5.75	2.10	7.47	9.23	27.38	23.55	6.410	5.560

Table 5: Performance of models against transfer-based *black box* attacks on *Hecktor* dataset.Figure 3: **Frequency Analysis (VAVA):** Low frequency components of adversarial perturbation cause significant performance degradation(DSC score is reported).

ing size n from the top left corner as part of the low-frequency components $(0, n)$ where $n \in \{8, 16, 32\}$. Similarly, mid-frequency $(16 - 48)$ and high-frequency $(16 - 96)$ components are also extracted. Our results as shown in Figure 3, show that across all models, the performance drop in adversarial perturbations crafted by VAVA is attributed to their low-frequency components. This finding deviates from previous studies in the natural domain [8, 24], which demonstrate that high-frequency components are linked to a decrease in performance. Our results align with recent works [28, 56] which suggest that the potency of adversarial examples cannot be solely attributed to high-frequency components. Instead, it depends on various factors including the model architecture and the characteristics of the dataset. We provide further frequency analysis across different attacks in the Appendix E.

4.4 Robustness of SAM-Med3D against Black-box Attacks

We assess the robustness of the SAM-Med3D model against adversarial examples crafted by different surrogate models. In Figure 4, we report the DSC score obtain by SAM-Med3D on different datasets. Similar to Section 4.2, we observe that adversarial examples crafted using pixel-based attacks do not transfer to SAM-Med3D, while adversarial examples crafted using VAVA exhibit greater transferability. However, in general, we observe that the drop

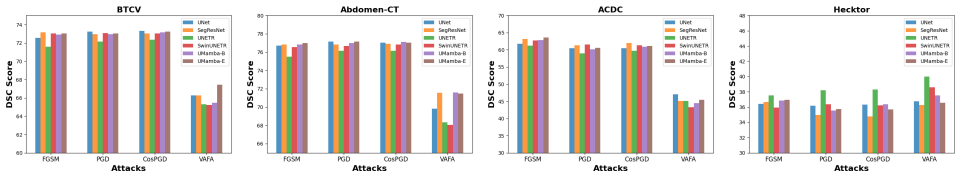


Figure 4: Evaluating SAM-Med3D against transfer-based *black box* attacks.

in performance of SAM-Med3D against transfer-based attacks is low compared to models trained on individual datasets(see Section 4.2), which can be attributed to the robust generalization capabilities of the model, which are attained through effective training on large-scale datasets. We report detailed results on SAM-Med3D in Appendix F.

5 Conclusion

This work presents the first comprehensive empirical study on the robustness of current volumetric medical segmentation models against adversarial attacks. Our results indicate that current pixel-based attacks while successful under *white box* settings show limited transferability to unknown target models. In contrast, frequency-based attacks result in highly transferable adversarial examples. We show that low-frequency changes to images in frequency-based attacks are responsible for the attack success. Across different models, we observe transformer-based models are more robust than CNNs and Mamba-based models under different adversarial settings. Moreover, we highlight the enhanced robustness of vision foundational models trained on large-scale datasets. Our study highlights the importance of evaluating the robustness of vision-based models in the medical field. We hope this will foster future efforts to improve the robustness of these models.

References

- [1] Shashank Agnihotri, Steffen Jung, and Margret Keuper. Cospgd: A unified white-box adversarial attack for pixel-wise prediction tasks. *arXiv preprint arXiv:2302.02213*, 2023.
- [2] Vincent Andrearczyk, Valentin Oreiller, Sarah Boughdad, Catherine Cheze Le Rest, Hesham Elhalawani, Mario Jreige, John O Prior, Martin Vallières, Dimitris Visvikis, Mathieu Hatt, et al. Overview of the hecker challenge at miccai 2021: automatic head and neck tumor segmentation and outcome prediction in pet/ct images. In *3D head and neck tumor segmentation in PET/CT challenge*, pages 1–37. Springer, 2021.
- [3] Yutong Bai, Jieru Mei, Alan L Yuille, and Cihang Xie. Are transformers more robust than cnns? *Advances in neural information processing systems*, 34:26831–26843, 2021.
- [4] Philipp Benz, Soomin Ham, Chaoning Zhang, Adil Karjauv, and In So Kweon. Adversarial robustness comparison of vision transformer and mlp-mixer to cnns. *arXiv preprint arXiv:2110.02797*, 2021.

- [5] Olivier Bernard, Alain Lalande, Clement Zotti, Frederick Cervenansky, Xin Yang, Pheng-Ann Heng, Irem Cetin, Karim Lekadir, Oscar Camara, Miguel Angel Gonzalez Ballester, et al. Deep learning techniques for automatic mri cardiac multi-structures segmentation and diagnosis: is the problem solved? *IEEE transactions on medical imaging*, 37(11):2514–2525, 2018.
- [6] Wieland Brendel, Jonas Rauber, and Matthias Bethge. Decision-based adversarial attacks: Reliable attacks against black-box machine learning models. In *International Conference on Learning Representations (ICLR)*, 2018.
- [7] Nicholas Carlini and David Wagner. Towards evaluating the robustness of neural networks. In *2017 IEEE Symposium on Security and Privacy (SP)*, pages 39–57. Ieee, 2017.
- [8] Guo Chen, Yifei Huang, Jilan Xu, Baoqi Pei, Zhe Chen, Zhiqi Li, Jiahao Wang, Kun-chang Li, Tong Lu, and Limin Wang. Video mamba suite: State space model as a versatile alternative for video understanding. *arXiv preprint arXiv:2403.09626*, 2024.
- [9] Jieneng Chen, Yongyi Lu, Qihang Yu, Xiangde Luo, Ehsan Adeli, Yan Wang, Le Lu, Alan L Yuille, and Yuyin Zhou. Transunet: Transformers make strong encoders for medical image segmentation. *arXiv preprint arXiv:2102.04306*, 2021.
- [10] Pin-Yu Chen, Huan Zhang, Yash Sharma, Jinfeng Yi, and Cho-Jui Hsieh. Zoo: Zeroth order optimization based black-box attacks to deep neural networks without training substitute models. In *Proceedings of the 10th ACM workshop on artificial intelligence and security*, 2017.
- [11] Francesco Croce and Matthias Hein. Reliable evaluation of adversarial robustness with an ensemble of diverse parameter-free attacks. In *International conference on machine learning*, pages 2206–2216. PMLR, 2020.
- [12] Laura Daza, Juan C Pérez, and Pablo Arbeláez. Towards robust general medical image segmentation. In *Medical Image Computing and Computer Assisted Intervention–MICCAI 2021: 24th International Conference, Strasbourg, France, September 27–October 1, 2021, Proceedings, Part III 24*, pages 3–13. Springer, 2021.
- [13] Yinpeng Dong, Fangzhou Liao, Tianyu Pang, Hang Su, Jun Zhu, Xiaolin Hu, and Jian-guo Li. Boosting adversarial attacks with momentum. In *Proceedings of the IEEE/CVF Conference on Computer Vision and Pattern Recognition (CVPR)*, 2018.
- [14] Alexey Dosovitskiy, Lucas Beyer, Alexander Kolesnikov, Dirk Weissenborn, Xiaohua Zhai, Thomas Unterthiner, Mostafa Dehghani, Matthias Minderer, Georg Heigold, Sylvain Gelly, et al. An image is worth 16x16 words: Transformers for image recognition at scale. *arXiv preprint arXiv:2010.11929*, 2020.
- [15] Ian J Goodfellow, Jonathon Shlens, and Christian Szegedy. Explaining and harnessing adversarial examples. *arXiv preprint arXiv:1412.6572*, 2014.
- [16] Albert Gu and Tri Dao. Mamba: Linear-time sequence modeling with selective state spaces. *arXiv preprint arXiv:2312.00752*, 2023.
- [17] Albert Gu, Karan Goel, and Christopher Ré. Efficiently modeling long sequences with structured state spaces. *arXiv preprint arXiv:2111.00396*, 2021.

- [18] Jindong Gu, Hengshuang Zhao, Volker Tresp, and Philip HS Torr. Segpgd: An effective and efficient adversarial attack for evaluating and boosting segmentation robustness. In *European Conference on Computer Vision*, pages 308–325. Springer, 2022.
- [19] Asif Hanif, Muzammal Naseer, Salman Khan, Mubarak Shah, and Fahad Shahbaz Khan. Frequency domain adversarial training for robust volumetric medical segmentation. In *International Conference on Medical Image Computing and Computer-Assisted Intervention*, pages 457–467. Springer, 2023.
- [20] Ali Hatamizadeh, Vishwesh Nath, Yucheng Tang, Dong Yang, Holger R Roth, and Daguang Xu. Swin unetr: Swin transformers for semantic segmentation of brain tumors in mri images. In *Brainlesion: Glioma, Multiple Sclerosis, Stroke and Traumatic Brain Injuries: 7th International Workshop, BrainLes 2021, Held in Conjunction with MICCAI 2021, Virtual Event, September 27, 2021, Revised Selected Papers, Part I*, pages 272–284. Springer, 2022.
- [21] Ali Hatamizadeh, Yucheng Tang, Vishwesh Nath, Dong Yang, Andriy Myronenko, Bennett Landman, Holger R Roth, and Daguang Xu. Unetr: Transformers for 3d medical image segmentation. In *Proceedings of the IEEE/CVF Winter Conference on Applications of Computer Vision*, pages 574–584, 2022.
- [22] Kaiming He, Xiangyu Zhang, Shaoqing Ren, and Jian Sun. Deep residual learning for image recognition. In *Proceedings of the IEEE conference on computer vision and pattern recognition*, pages 770–778, 2016.
- [23] Fabian Isensee, Tassilo Wald, Constantin Ulrich, Michael Baumgartner, Saikat Roy, Klaus Maier-Hein, and Paul F Jaeger. nnu-net revisited: A call for rigorous validation in 3d medical image segmentation. *arXiv preprint arXiv:2404.09556*, 2024.
- [24] Xiaojun Jia, Jindong Gu, Yihao Huang, Simeng Qin, Qing Guo, Yang Liu, and Xiaochun Cao. Transegpgd: Improving transferability of adversarial examples on semantic segmentation. *arXiv preprint arXiv:2312.02207*, 2023.
- [25] Alexey Kurakin, Ian Goodfellow, and Samy Bengio. Adversarial machine learning at scale. *arXiv preprint arXiv:1611.01236*, 2016.
- [26] Alexey Kurakin, Ian J Goodfellow, and Samy Bengio. Adversarial examples in the physical world. In *Artificial intelligence safety and security*, pages 99–112. Chapman and Hall/CRC, 2018.
- [27] Bennett Landman, Zhoubing Xu, J Igelsias, Martin Styner, Thomas Langerak, and Arno Klein. Miccai multi-atlas labeling beyond the cranial vault—workshop and challenge. In *Proc. MICCAI Multi-Atlas Labeling Beyond Cranial Vault—Workshop Challenge*, volume 5, page 12, 2015.
- [28] Chen Li, Yong Liu, Xinpeng Zhang, and Hanzhou Wu. Exploiting frequency characteristics for boosting the invisibility of adversarial attacks. *Applied Sciences*, 14(8):3315, 2024.
- [29] Kunchang Li, Xinhao Li, Yi Wang, Yanan He, Yali Wang, Limin Wang, and Yu Qiao. Videomamba: State space model for efficient video understanding. *arXiv preprint arXiv:2403.06977*, 2024.

- [30] Yue Liu, Yunjie Tian, Yuzhong Zhao, Hongtian Yu, Lingxi Xie, Yaowei Wang, Qixiang Ye, and Yunfan Liu. Vmamba: Visual state space model. *arXiv preprint arXiv:2401.10166*, 2024.
- [31] Ze Liu, Yutong Lin, Yue Cao, Han Hu, Yixuan Wei, Zheng Zhang, Stephen Lin, and Baining Guo. Swin transformer: Hierarchical vision transformer using shifted windows. In *Proceedings of the IEEE/CVF international conference on computer vision*, pages 10012–10022, 2021.
- [32] Wenjie Luo, Yujia Li, Raquel Urtasun, and Richard Zemel. Understanding the effective receptive field in deep convolutional neural networks. *Advances in neural information processing systems*, 29, 2016.
- [33] Jun Ma, Yao Zhang, Song Gu, Cheng Zhu, Cheng Ge, Yichi Zhang, Xingle An, Congcong Wang, Qiyuan Wang, Xin Liu, et al. Abdomenct-1k: Is abdominal organ segmentation a solved problem? *IEEE Transactions on Pattern Analysis and Machine Intelligence*, 44(10):6695–6714, 2021.
- [34] Jun Ma, Feifei Li, and Bo Wang. U-mamba: Enhancing long-range dependency for biomedical image segmentation. *arXiv preprint arXiv:2401.04722*, 2024.
- [35] Aleksander Madry, Aleksandar Makelov, Ludwig Schmidt, Dimitris Tsipras, and Adrian Vladu. Towards deep learning models resistant to adversarial attacks. *arXiv preprint arXiv:1706.06083*, 2017.
- [36] Shishira R Maiya, Max Ehrlich, Vatsal Agarwal, Ser-Nam Lim, Tom Goldstein, and Abhinav Shrivastava. A frequency perspective of adversarial robustness. *arXiv preprint arXiv:2111.00861*, 2021.
- [37] Hashmat Shadab Malik, Shahina K Kunhimon, Muzammal Naseer, Salman Khan, and Fahad Shahbaz Khan. Adversarial pixel restoration as a pretext task for transferable perturbations. *arXiv preprint arXiv:2207.08803*, 2022.
- [38] Andriy Myronenko. 3d mri brain tumor segmentation using autoencoder regularization. In *Brainlesion: Glioma, Multiple Sclerosis, Stroke and Traumatic Brain Injuries: 4th International Workshop, BrainLes 2018, Held in Conjunction with MICCAI 2018, Granada, Spain, September 16, 2018, Revised Selected Papers, Part II 4*, pages 311–320. Springer, 2019.
- [39] Nina Narodytska and Shiva Kasiviswanathan. Simple black-box adversarial attacks on deep neural networks. In *Computer Vision and Pattern Recognition (CVPR) Workshop*, 2017.
- [40] Muhammad Muzammal Naseer, Salman H Khan, Muhammad Haris Khan, Fahad Shahbaz Khan, and Fatih Porikli. Cross-domain transferability of adversarial perturbations. *Advances in Neural Information Processing Systems (NeurIPS)*, 2019.
- [41] Muhammad Muzammal Naseer, Kanchana Ranasinghe, Salman H Khan, Munawar Hayat, Fahad Shahbaz Khan, and Ming-Hsuan Yang. Intriguing properties of vision transformers. *Advances in Neural Information Processing Systems*, 34:23296–23308, 2021.

- [42] Francesco Pinto, Philip HS Torr, and Puneet K. Dokania. An impartial take to the cnn vs transformer robustness contest. In *European Conference on Computer Vision*, pages 466–480. Springer, 2022.
- [43] Olaf Ronneberger, Philipp Fischer, and Thomas Brox. U-net: Convolutional networks for biomedical image segmentation. In Nassir Navab, Joachim Hornegger, William M. Wells, and Alejandro F. Frangi, editors, *Medical Image Computing and Computer-Assisted Intervention – MICCAI 2015*, pages 234–241, Cham, 2015. Springer International Publishing. ISBN 978-3-319-24574-4.
- [44] Rulin Shao, Zhouxing Shi, Jinfeng Yi, Pin-Yu Chen, and Cho-Jui Hsieh. On the adversarial robustness of vision transformers. *arXiv preprint arXiv:2103.15670*, 2021.
- [45] Karen Simonyan and Andrew Zisserman. Very deep convolutional networks for large-scale image recognition. *arXiv preprint arXiv:1409.1556*, 2014.
- [46] Jiawei Su, Danilo Vasconcellos Vargas, and Kouichi Sakurai. One pixel attack for fooling deep neural networks. *IEEE Transactions on Evolutionary Computation*, 23(5):828–841, 2019.
- [47] Carole H Sudre, Wenqi Li, Tom Vercauteren, Sebastien Ourselin, and M Jorge Cardoso. Generalised dice overlap as a deep learning loss function for highly unbalanced segmentations. In *Deep Learning in Medical Image Analysis and Multimodal Learning for Clinical Decision Support: Third International Workshop, DLMIA 2017, Québec City, QC, Canada, September 14, Proceedings 3*, pages 240–248. Springer, 2017.
- [48] Christian Szegedy, Wojciech Zaremba, Ilya Sutskever, Joan Bruna, Dumitru Erhan, Ian Goodfellow, and Rob Fergus. Intriguing properties of neural networks. *arXiv preprint arXiv:1312.6199*, 2013.
- [49] Hugo Touvron, Matthieu Cord, Matthijs Douze, Francisco Massa, Alexandre Sablayrolles, and Hervé Jégou. Training data-efficient image transformers & distillation through attention. In *International conference on machine learning*, pages 10347–10357. PMLR, 2021.
- [50] Haoyu Wang, Sizheng Guo, Jin Ye, Zhongying Deng, Junlong Cheng, Tianbin Li, Jianpin Chen, Yanzhou Su, Ziyang Huang, Yiqing Shen, et al. Sam-med3d. *arXiv preprint arXiv:2310.15161*, 2023.
- [51] Richard Zhang, Phillip Isola, Alexei A Efros, Eli Shechtman, and Oliver Wang. The unreasonable effectiveness of deep features as a perceptual metric. In *Proceedings of the IEEE conference on computer vision and pattern recognition*, pages 586–595, 2018.
- [52] Lianghui Zhu, Bencheng Liao, Qian Zhang, Xinlong Wang, Wenyu Liu, and Xinggang Wang. Vision mamba: Efficient visual representation learning with bidirectional state space model. *arXiv preprint arXiv:2401.09417*, 2024.

Appendix

We offer further insights into our study through various sections in the appendix. Firstly, we provide additional details regarding the datasets utilized in Section A and elaborate on the training recipe for the models, as discussed in Section B. In Section C, we delve deeper into the *white box* analysis, providing ablations across all datasets, examining pixel and frequency-based attacks at different perturbation budgets. Likewise, Section E expands on the frequency analysis initially presented in Section 4.3, covering different adversarial attacks. Lastly, in Section F, we present results on transfer-based *black box* attacks across all datasets, considering various perturbation strengths, and offer further insights derived from these findings. **Our well-documented code and pretrained weights will be made publicly available.**

A Datasets

Medical imaging data sets encompass a range of imaging techniques, including Positron Emission Tomography (PET), Computed Tomography (CT), and Magnetic Resonance Imaging (MRI). PET scans effectively show the metabolic or biochemical activity within the body, and CT imaging offers high-resolution images of the body’s internal structure. Similarly, MRIs effectively differentiate between soft tissues without the use of ionizing radiation. These imaging modalities acquire comprehensive and complementary information about the body’s organs, functions, and tumors. Thus, to conduct a comprehensive benchmarking analysis of the model’s robustness and susceptibility to adversarial attacks, we utilize four different segmentation datasets: *BTCV*, *ACDC*, *Hecktor*, and *Abdomen-CT*, which consist of medical images from CT and MRI modalities encompassing different tumor and organ segmentations.

BTCV: The *BTCV* dataset consists of 30 abdominal CT scans from metastatic liver cancer patients acquired from a single medical center. Each CT scan is manually annotated for 13 abdominal organs (Spleen, Right Kidney, Left Kidney, Gallbladder, Esophagus, Liver, Stomach, Aorta, IVC, Portal and Splenic Veins, Pancreas, Right adrenal gland, and Left adrenal gland). The CT scan size is 512×512 pixels, the number of slices ranges from 80 to 225, and the slice thickness ranges from 1 to 6 mm.

ACDC: The Automated Cardiac Diagnosis Challenge (*ACDC*) dataset consists of 150 MRI images from patients with cardiac abnormalities acquired from a single medical center. Each MRI scan is manually annotated for different heart organs, such as the left ventricle (LV), right ventricle (RV), and myocardium (MYO). The number of MRI slices ranges from 28 to 40, and the slice thickness ranges from 5 to 8 mm. The spatial resolution goes from 1.37 to $1.68 \text{ mm}^2/\text{pixel}$.

HECKTOR: The *Hecktor* dataset consists of 524 CT/PET scans of head and neck cancer patients collected from seven medical centers. It was manually annotated for primary gross tumor volumes (GTVp) and nodal gross tumor volumes (GTVn). The CT scan size ranges from 128×128 to 512×512 , the number of slices ranges from 67 to 736, and the slice thickness ranges from 1 to 2.8 mm.

AbdomenCT-1k: The *AbdomenCT-1k* dataset consists of 1112 abdominal CT scans from 12 medical centers, including multi-phase, multi-vendor, and multi-disease cases. All the scans’ annotations for the liver, kidney, spleen, and pancreas are provided. The CT scan size

has resolutions of 512×512 pixels with varying voxel sizes and slice thicknesses between 1.25 to 5 mm.

B Training Details

For `BTCV`, `Abdomen-CT`, and `ACDC` all models trained for 5000 epochs, while for `Hecktor` we use only 500 epochs. A batch size of 3 and a learning rate (`lr`) of $1e-4$ with the `warmup_cosine` scheduler is used. During training, images are normalized to the range of $[0, 1]$, and a 3D random crop of size $96 \times 96 \times 96$ is selected as an input to the segmentation model. Augmentations include `RandomFlip` (for all three spatial dimensions), `RandomRotate90`, `RandomScaleIntensity`, and `RandomShiftIntensity`. During inference, we employed a sliding window approach, dividing the input volume of arbitrary size into 3D sliding windows of size $96 \times 96 \times 96$ with a 50% overlap. The predictions of overlapping voxels were combined using a Gaussian kernel.

C Robustness against White-box Attacks

In Figure 5, we report robustness of the volumetric segmentation models on *white box* attacks across `BTCV`, `Abdomen-CT`, `Hecktor`, and `ACDC` datasets. For pixel-based attacks we craft adversarial examples at l_∞ perturbation budget $\epsilon \in \{\frac{4}{255}, \frac{8}{255}\}$ for `FGSM`, `PGD`, and `CosPGD`. For frequency-based attack `VAVA` we craft adversarial examples with $q_{max} \in \{10, 30\}$. We report DSC and LPIPS score on generated adversarial examples. Similar to our results in Table 1 in the main paper, we observe that `VAVA` causes the most drop in DSC score of models on `BTCV` and `Abdomen-CT` dataset, while iterative pixel-based attacks `PGD` and `CosPGD` cause the most drop on `Hecktor` and `ACDC` dataset. Furthermore, we provide ablation across `VAVA` attack with varying $q_{max} \in \{10, 20, 30\}$ in Figure 6. With an increase in q_{max} , we observe a decrease in the DSC score across all the datasets. Consequently, we also observe a drop in the LPIPS score of the generated adversarial examples.

D Adversarial Examples

In Figure 7, adversarial example using `VAVA` is crafted on `UNet` model trained on `Abdomen-CT` dataset. Segmentation prediction of all the volumetric segmentation models is shown for the clean sample and the adversarial one. We can clearly observe that the adversarial example causes the predictions to change across all models.

E Frequency Analysis of White-Box Attacks

In this section, we delve deeper into the frequency analysis of adversarial attacks to study which frequency components lead to drop in performance of models. Following [14], we implement an adversarial attack incorporating a frequency filter M , restricting perturbations to specific frequency domains. The filter operation is defined as $x'_{freq} = \text{IDCT}(\text{DCT}(x' - x) \odot M) + x$, where `DCT` and `IDCT` denote Discrete Cosine Transform and its inverse, respectively. Similar to [14], using the filter M , we extract 3D cubes of varying size n from the top left corner as part of the low-frequency components $(0, n)$ where $n \in \{8, 16, 32\}$. Similarly, mid-frequency

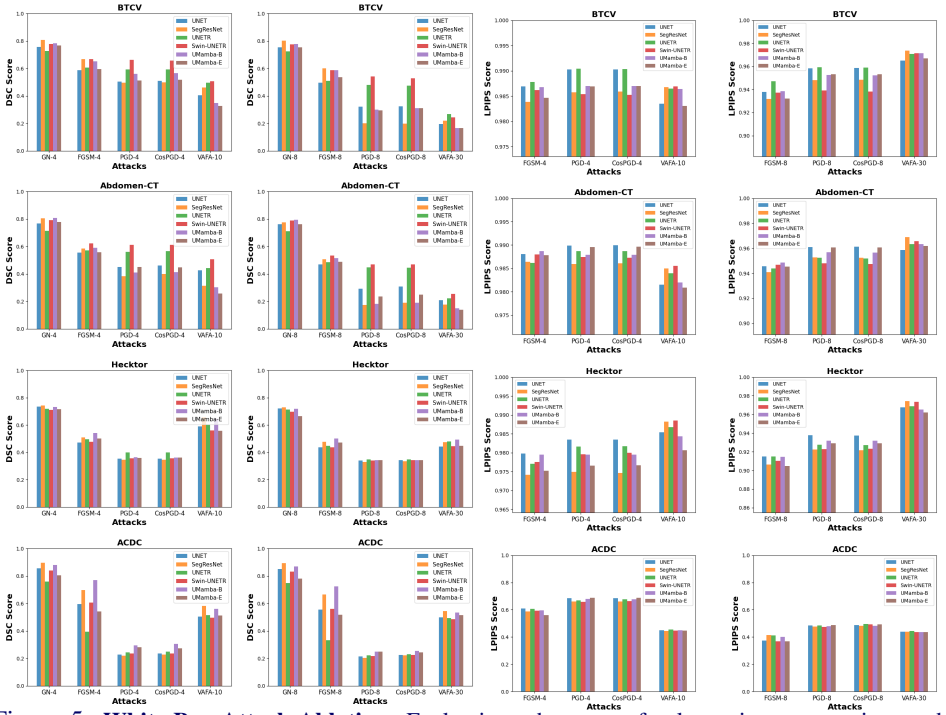


Figure 5: **White Box Attack Ablation:** Evaluating robustness of volumetric segmentation models on *white box* attacks. For pixel-based attacks results are reported for $\varepsilon = \frac{4}{255}$ and $\varepsilon = \frac{8}{255}$ indicated by attack names followed by the suffixes -4 or -8 , respectively. Regarding frequency-based attack VAFA, the results are reported with a constraint on q_{\max} set to 10 and 30, denoted as VAFA-10 and VAFA-30, respectively. DSC score (*lower is better*) and LPIPS score (*higher is better*) are reported on the generated adversarial examples.

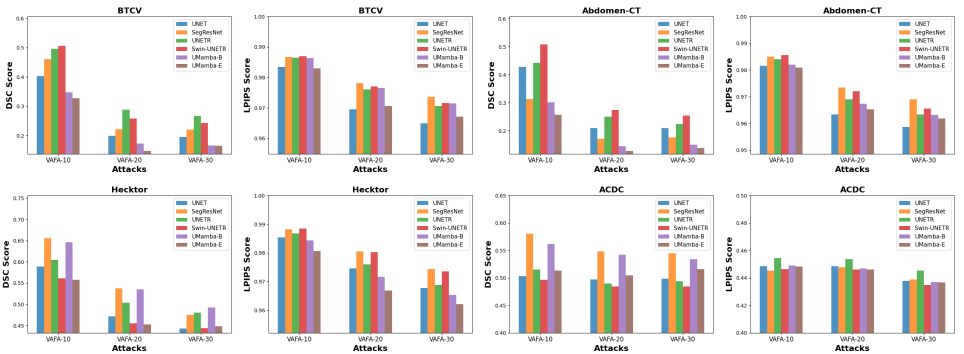


Figure 6: **Frequency Attack Ablation:** Examining the robustness of volumetric segmentation models VAFA based *white box* attack. Adversarial examples are generated at $q_{\max} \in \{10, 20, 30\}$, represented as VAFA-10, VAFA-20, and VAFA-30, respectively. DSC score (*lower is better*) and LPIPS score (*higher is better*) are reported on the generated adversarial examples.

(16 – 48) and high-frequency (16 – 96) components are also extracted. See Figure 8 for the design of filters. While in Figure 3 of the main paper, we provide frequency analysis on VAFA, which shows the best transferability across target models. Figure 9 expands this anal-

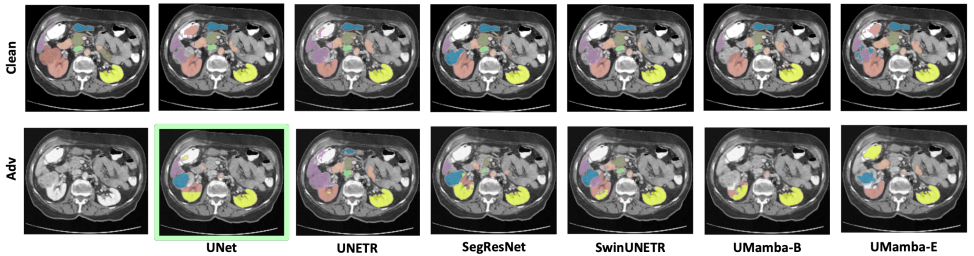


Figure 7: Comparing multi-organ segmentation across various models under transfer-based *black box* attacks, where adversarial examples are generated on UNet and transferred to other unseen models.

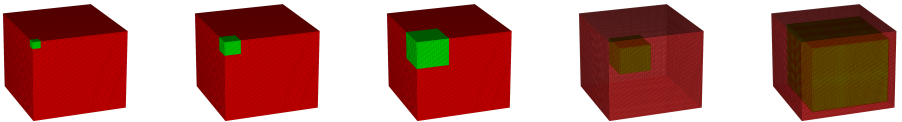


Figure 8: **Frequency Analysis Filters:** The frequencies associated with the red section are eliminated, while those linked to the green section are allowed to pass. These filters are labeled as $(0-8)$, $(0-16)$, $(0-32)$, $(16-48)$, and $(16-96)$ (from right to left).

ysis to encompass all the adversarial attacks employed in our experiments. For pixel-based attacks, we report results at $\varepsilon = \frac{8}{255}$ and for VAFA at $q_{max} = 30$. In the case of the VAFA attack, which demonstrates significant *transferability* to the target models in *black box* setting, we note that the low-frequency components of the adversarial examples predominantly contribute to the performance decline across surrogate volumetric segmentation models. While a similar trend is observed with pixel-based attacks, it is not as pronounced as with VAFA. For instance, when analyzing the Abdomen-CT and ACDC datasets, we find that the high-frequency components of adversarial examples generated by pixel-based attacks also result in a noticeable performance decrease across models. However, as discussed in Section 4.2, these adversarial examples produced by pixel-based attacks exhibit very limited transferability.

F Robustness against Black-box Attacks

In Tables 6, 7, 8, and 9, we report robustness of the volumetric segmentation models on *black box* attacks across BTCV, Abdomen-CT, Hecktor, and ACDC datasets. For pixel-based attacks we craft adversarial examples at l_∞ perturbation budget $\varepsilon = \frac{4}{255}$ for FGSM, PGD, and CosPGD. For frequency-based attack VAFA we craft adversarial examples with $q_{max} = 20$. We report DSC and LPIPS score on generated adversarial examples. Similar to our observations for $\varepsilon = \frac{8}{255}$ and $q_{max} = 30$ in Section 4.2, we observe frequency-based attack VAFA results in significant transferability of adversarial examples to target models at $\varepsilon = \frac{4}{255}$ and $q_{max} = 20$ as well. Further, we also report the DSC and HD95 score for results reported in Section 4.2 of the main paper in Table 10, 11, 12, and 13. Finally, in Table 14, we report performance of SAM-Med3D on adversarial examples crafted on surrogate models trained on BTCV, Abdomen-CT, Hecktor, and ACDC datasets.

We believe our empirical results showing higher transferability obtained from frequency

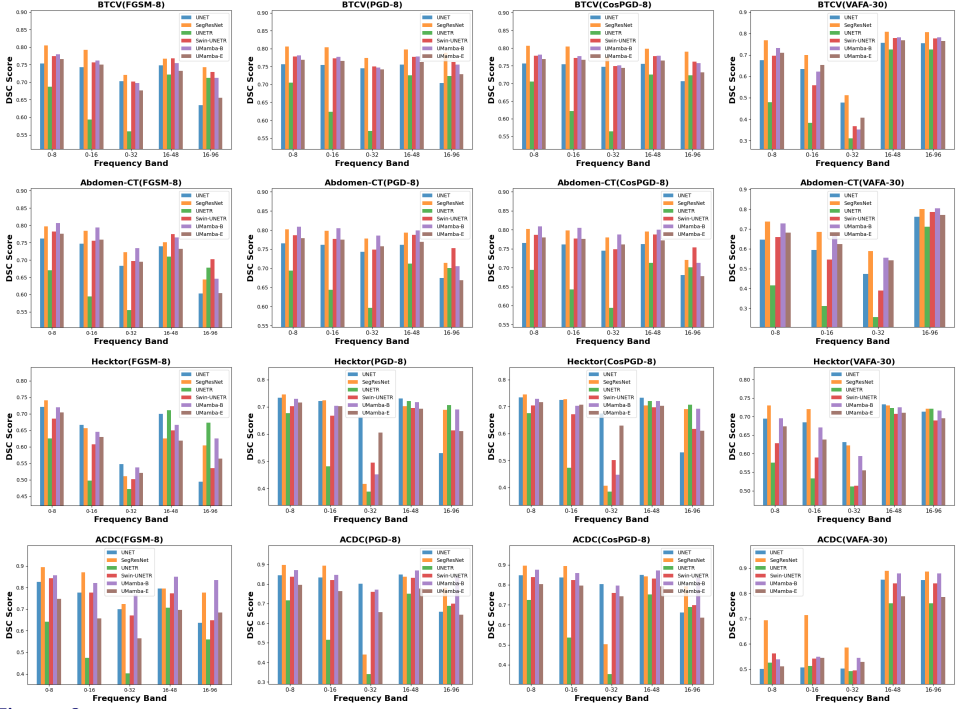


Figure 9: **Frequency Analysis on FGSM, PGD, CosPGD, and VAVA:** We report the performance drop on models in *white box* settings across adversarial attacks. We restrict the adversarial perturbations to be added to the image within different frequency ranges. For pixel-based attacks results are reported for $\epsilon = \frac{8}{255}$ indicated by attack names followed by the suffixes -8 , respectively. Regarding frequency-based attack VAVA, the results are reported with a constraint on q_{\max} set to 30, denoted as VAVA-30. DSC score (*lower is better*) is reported on the generated adversarial examples.

domain attack can be attributed to the ability of frequency domain perturbations to affect a wider range of model architectures and training datasets compared to spatial domain perturbations. One possible reason for the higher transferability obtained from frequency domain adversarial attacks is that frequency domain perturbations can capture more abstract and general features of the input data. These perturbations may affect the underlying patterns and structures that are common across different models and datasets, making them more transferable across various scenarios. Additionally, frequency domain transformations can be less sensitive to small changes in pixel values, leading to more robust and consistent adversarial examples across different scenarios.

Surrogate	Attack	UNet		SegResNet		UNETR		SwinUNETR		UMamba-B		UMamba-E	
		DSC↓	HD95↑	DSC↓	HD95↑	DSC↓	HD95↑	DSC↓	HD95↑	DSC↓	HD95↑	DSC↓	HD95↑
	Clean	75.72	9.15	80.84	8.14	72.53	15.08	78.07	10.01	78.37	8.12	77.06	11.11
	GN	75.65	9.69	80.72	8.37	72.66	14.72	77.88	9.98	78.24	8.18	76.68	16.04
UNet	FGSM-4	58.77	37.71	79.6	8.36	71.72	14.72	76.7	10.39	76.85	9.4	75.18	15.44
	PGD-4	50.53	53.9	80.42	8.51	72.42	14.68	77.57	10.21	77.7	8.69	76.22	14.28
	CosPGD-4	50.97	48.99	80.4	8.49	72.37	14.78	77.57	10.18	77.66	8.57	76.26	14.53
	VAFa-20	56.13	39.73	69.69	18.68	53.19	31.66	66.8	28.34	72.53	14.38	69.63	15.5
SegResNet	FGSM-4	74.0	10.75	66.68	32.41	71.45	15.21	75.27	10.69	73.33	11.1	72.95	15.6
	PGD-4	74.57	13.03	49.49	65.31	71.83	15.25	76.67	10.45	74.96	11.63	73.97	16.1
	CosPGD-4	74.51	13.02	49.89	60.42	71.78	15.45	76.64	10.47	74.99	11.41	73.85	16.77
	VAFa-20	61.59	20.73	51.44	37.74	43.33	41.75	58.62	28.87	68.92	13.88	66.03	17.45
UNETR	FGSM-4	73.68	9.95	79.08	8.72	60.52	32.3	75.12	10.79	76.02	8.82	74.91	12.88
	PGD-4	74.34	11.04	79.8	8.54	59.27	36.6	76.27	10.48	76.83	9.08	75.47	11.66
	CosPGD-4	74.29	10.62	79.79	8.43	59.17	38.39	76.29	10.48	76.83	9.05	75.35	12.85
	VAFa-20	55.31	26.62	57.5	23.07	35.09	45.42	50.44	30.85	63.53	17.54	59.1	21.81
SwinUNETR	FGSM-4	73.91	11.86	78.36	9.34	70.89	15.55	66.8	24.71	75.41	9.41	74.37	13.14
	PGD-4	74.22	12.24	79.47	9.24	71.45	15.96	66.37	32.63	76.36	10.24	75.21	16.84
	CosPGD-4	74.24	12.22	79.4	9.24	71.43	15.96	65.82	32.86	76.37	10.22	75.09	19.19
	VAFa-20	59.36	24.77	61.67	26.59	47.41	40.06	54.22	45.64	65.13	17.85	62.44	21.08
UMamba-B	FGSM-4	73.81	13.17	76.57	11.88	71.52	14.8	75.39	10.84	65.17	24.69	71.63	20.33
	PGD-4	74.69	11.6	78.78	10.44	71.92	15.03	76.88	10.58	56.03	47.41	73.43	19.04
	CosPGD-4	74.56	11.52	78.7	11.24	71.88	15.13	76.85	10.54	56.53	45.15	73.18	19.13
	VAFa-20	73.3	14.16	76.82	10.92	67.21	16.77	74.83	14.62	68.22	19.06	73.58	15.0
UMamba-E	FGSM-4	74.34	10.36	78.49	10.11	71.69	15.08	76.37	10.56	75.04	11.29	59.47	36.77
	PGD-4	75.2	10.54	80.34	8.6	72.31	14.89	77.71	10.29	77.41	10.21	51.3	57.83
	CosPGD-4	75.23	12.35	80.28	9.36	72.31	14.74	77.62	10.26	77.33	10.1	51.67	54.16
	VAFa-20	73.74	13.94	78.67	10.6	68.15	13.88	75.36	16.89	77.09	8.56	62.15	38.97

Table 6: Performance of models against transfer-based *black box* attacks on BTCV dataset. For pixel-based attacks results are reported for $\epsilon = \frac{4}{255}$ indicated by attack names followed by the suffixes -4, respectively. Regarding frequency-based attack VAFa, the results are reported with a constraint on q_{\max} set to 20, denoted as VAFa-20. DSC score (*lower is better*) is reported on the generated adversarial examples.

Surrogate	Attack	UNet		SegResNet		UNETR		SwinUNETR		UMamba-B		UMamba-E	
		DSC↓	HD95↑	DSC↓	HD95↑	DSC↓	HD95↑	DSC↓	HD95↑	DSC↓	HD95↑	DSC↓	HD95↑
	Clean	76.79	19.72	80.89	13.30	71.35	27.73	79.33	25.79	81.08	15.51	78.05	18.31
UNet	FGSM-4	55.49	49.07	77.63	14.51	70.19	31.9	77.31	28.89	77.51	18.02	74.69	18.88
	PGD-4	45.11	60.73	78.86	14.2	70.78	32.96	78.49	27.38	79.26	18.67	76.37	17.3
	CosPGD-4	46.15	56.43	78.92	13.65	70.78	32.49	78.48	27.06	79.38	16.8	76.49	17.09
	VAFa-20	20.98	79.82	25.59	64.99	39.1	65.7	38.01	60.38	22.87	69.81	17.97	72.59
SegResNet	FGSM-4	73.99	21.52	58.49	40.26	70.12	32.88	76.92	26.18	73.01	22.27	71.63	19.58
	PGD-4	75.32	21.71	38.38	76.59	70.74	32.11	78.1	27.63	76.2	18.0	74.31	19.26
	CosPGD-4	75.28	21.9	39.99	71.41	70.73	31.93	78.09	28.11	76.09	20.27	74.31	18.12
	VAFa-20	37.16	48.6	17.07	86.27	45.66	48.14	43.38	50.99	22.17	66.08	17.25	72.17
UNETR	FGSM-4	74.07	21.03	77.61	14.12	57.17	47.62	75.8	27.04	77.75	19.74	74.62	18.03
	PGD-4	74.88	21.39	78.53	14.16	56.09	54.17	77.06	27.34	78.7	18.36	75.46	17.04
	CosPGD-4	74.9	21.2	78.62	14.25	56.47	51.35	77.14	26.5	78.76	17.46	75.59	16.86
	VAFa-20	41.79	51.35	33.3	54.93	25.07	81.29	39.73	54.54	29.44	55.98	27.03	55.56
SwinUNETR	FGSM-4	73.67	21.14	76.4	15.09	69.15	32.35	62.36	53.75	76.46	18.36	73.79	19.52
	PGD-4	74.7	22.26	77.75	14.97	69.93	35.14	61.12	62.08	78.21	17.08	75.29	18.76
	CosPGD-4	74.74	21.24	77.81	15.17	69.95	33.62	61.11	59.67	78.14	16.96	75.3	18.39
	VAFa-20	31.55	58.31	27.55	59.83	35.04	61.92	27.41	72.71	24.01	65.52	21.14	68.78
UMamba-B	FGSM-4	73.88	23.47	73.57	17.24	70.06	33.54	76.92	27.25	59.06	45.82	70.01	25.71
	PGD-4	75.23	21.66	76.18	16.31	70.71	32.94	78.15	27.58	41.0	72.28	72.81	21.73
	CosPGD-4	75.14	22.07	76.19	16.21	70.71	32.76	78.13	26.97	41.31	73.11	72.87	21.47
	VAFa-20	37.29	55.72	22.86	65.32	45.02	57.95	43.66	52.85	14.45	91.51	17.12	76.75
UMamba-E	FGSM-4	74.1	21.44	75.43	15.89	70.08	33.24	77.17	27.36	73.23	21.73	55.75	46.17
	PGD-4	75.58	21.91	77.85	15.16	70.86	32.12	78.45	27.14	76.53	18.44	45.08	64.08
	CosPGD-4	75.54	21.46	77.77	15.09	70.82	32.04	78.44	27.76	76.72	18.25	44.7	59.92
	VAFa-20	38.54	54.64	25.12	64.86	45.39	60.19	45.1	53.93	22.68	72.02	12.76	93.07

Table 7: Performance of models against transfer-based *black box* attacks on Abdomen-CT dataset. For pixel-based attacks results are reported for $\epsilon = \frac{4}{255}$ indicated by attack names followed by the suffixes -4, respectively. Regarding frequency-based attack VAFa, the results are reported with a constraint on q_{\max} set to 20, denoted as VAFa-20. DSC score (*lower is better*) is reported on the generated adversarial examples.

Surrogate	Attack	UNet		SegResNet		UNETR		SwinUNETR		UMamba-B		UMamba-E	
		DSC↓	HD95↑	DSC↓	HD95↑	DSC↓	HD95↑	DSC↓	HD95↑	DSC↓	HD95↑	DSC↓	HD95↑
	Clean	73.91	11.36	74.73	11.08	72.36	14.61	71.61	22.07	73.50	10.89	72.19	13.29
UNet	FGSM-4	47.09	34.93	66.43	14.93	69.56	15.36	64.99	27.04	66.4	13.95	64.54	15.78
	PGD-4	35.45	74.93	70.95	12.63	71.06	15.5	68.1	25.57	69.56	12.38	68.93	14.33
	CosPGD-4	35.35	75.02	70.94	12.44	71.12	15.48	68.26	24.87	69.76	12.26	69.11	15.95
	VAFa-20	47.18	37.67	71.81	13.39	65.29	18.38	66.4	19.96	68.94	14.23	62.6	19.23
SegResNet	FGSM-4	65.95	19.65	51.08	29.89	70.11	16.15	63.28	29.1	60.19	19.86	61.2	21.39
	PGD-4	67.57	16.92	34.53	76.44	70.65	14.89	64.93	27.82	60.05	25.77	62.3	20.78
	CosPGD-4	68.18	16.59	34.44	76.67	70.78	14.84	65.21	27.15	60.25	24.63	62.28	18.18
	VAFa-20	70.06	17.43	53.74	26.07	66.36	17.73	65.13	23.35	67.99	14.94	63.06	21.2
UNETR	FGSM-4	65.86	16.76	67.22	13.6	49.69	28.51	62.87	28.55	66.27	13.45	64.41	15.66
	PGD-4	67.24	18.42	68.89	14.18	39.98	57.26	64.09	28.24	68.12	14.02	66.81	14.71
	CosPGD-4	67.62	18.51	68.9	14.62	39.97	58.22	64.41	27.93	68.09	14.1	66.77	15.9
	VAFa-20	66.46	16.01	71.08	13.66	50.4	30.36	58.58	26.82	66.81	15.32	59.47	22.95
SwinUNETR	FGSM-4	64.77	17.07	62.78	15.66	68.79	16.25	47.62	50.52	61.94	17.02	61.6	19.59
	PGD-4	64.77	20.54	63.71	17.34	69.26	17.86	35.71	71.66	63.03	19.62	62.32	19.43
	CosPGD-4	64.89	20.28	64.0	17.41	69.3	17.63	35.67	71.17	63.62	18.24	62.63	19.32
	VAFa-20	67.49	19.81	70.16	14.05	63.04	20.19	45.55	39.63	68.31	16.17	58.99	21.62
UMamba-B	FGSM-4	65.9	15.64	60.75	17.1	70.0	15.18	62.54	29.27	54.27	25.87	60.26	19.26
	PGD-4	68.38	15.01	57.51	27.59	71.01	15.12	64.41	28.32	36.54	73.08	59.32	23.49
	CosPGD-4	68.57	15.83	57.11	29.09	71.06	15.1	64.85	28.94	36.2	72.71	60.1	24.75
	VAFa-20	67.38	19.59	68.45	14.79	65.08	17.12	65.41	22.1	53.55	31.11	60.21	21.25
UMamba-E	FGSM-4	67.51	15.97	64.71	14.8	70.57	15.6	65.7	27.37	63.32	17.41	50.06	31.45
	PGD-4	71.99	12.47	71.35	12.6	71.57	14.44	69.5	23.35	70.11	13.39	35.94	74.19
	CosPGD-4	71.84	13.13	71.61	12.14	71.58	14.44	69.47	23.63	70.48	14.36	36.07	73.97
	VAFa-20	68.52	19.79	71.56	13.43	64.93	18.85	66.36	22.05	68.19	21.2	45.28	31.42

Table 8: Performance of models against transfer-based *black box* attacks on *Hecktor* dataset. For pixel-based attacks results are reported for $\epsilon = \frac{4}{255}$ indicated by attack names followed by the suffixes -4 , respectively. Regarding frequency-based attack VAFa, the results are reported with a constraint on q_{\max} set to 20, denoted as VAFa-20. DSC score (*lower is better*) is reported on the generated adversarial examples.

Surrogate	Attack	UNet		SegResNet		UNETR		SwinUNETR		UMamba-B		UMamba-E	
		DSC↓	HD95↑	DSC↓	HD95↑	DSC↓	HD95↑	DSC↓	HD95↑	DSC↓	HD95↑	DSC↓	HD95↑
	Clean	85.52	5.75	89.65	2.56	76.37	16.31	84.19	7.93	88.22	6.01	80.91	8.48
UNet	FGSM-4	59.57	18.93	88.54	3.74	75.15	17.32	82.86	8.27	86.93	7.05	79.17	8.92
	PGD-4	22.75	38.22	89.38	3.18	75.73	17.29	83.75	8.63	87.72	6.8	80.02	8.73
	CosPGD-4	23.52	35.54	89.24	3.29	75.46	17.34	83.5	8.48	87.72	6.4	79.95	8.55
	VAFa-20	49.69	27.47	74.0	17.66	55.71	22.52	58.27	22.96	60.81	24.13	52.7	25.48
SegResNet	FGSM-4	84.67	5.92	69.85	11.22	75.08	17.52	82.49	8.16	85.2	10.12	78.95	8.57
	PGD-4	85.04	6.09	21.96	38.44	75.62	17.08	83.62	8.24	87.42	6.84	80.03	8.77
	CosPGD-4	85.08	5.85	22.68	38.34	75.67	17.15	83.62	8.16	87.31	6.77	79.3	8.73
	VAFa-20	51.79	27.04	54.8	23.06	54.41	22.32	56.64	22.84	59.04	24.27	51.82	26.04
UNETR	FGSM-4	83.39	8.43	87.74	4.14	39.45	26.49	80.67	10.34	85.09	12.68	78.52	9.45
	PGD-4	85.01	7.95	88.31	4.25	24.3	33.77	82.93	9.62	86.46	11.63	78.72	9.19
	CosPGD-4	85.09	7.79	88.16	4.37	24.79	33.27	82.63	10.53	86.22	12.23	78.15	9.53
	VAFa-20	52.38	26.55	73.19	16.56	48.99	23.31	55.29	24.52	57.86	24.69	50.38	26.23
SwinUNETR	FGSM-4	84.44	6.38	85.64	4.41	74.37	16.69	60.68	19.26	84.64	8.6	78.99	8.58
	PGD-4	84.95	5.85	87.83	4.6	74.53	17.5	23.47	34.53	86.65	8.74	77.56	9.95
	CosPGD-4	85.0	6.39	87.92	3.96	74.46	17.59	23.54	34.97	86.78	8.84	77.86	9.68
	VAFa-20	51.47	26.55	70.59	16.1	53.55	22.66	48.42	25.2	57.92	24.72	51.46	26.11
UMamba-B	FGSM-4	83.68	8.65	86.22	4.41	74.71	17.35	82.2	8.95	76.9	14.19	77.72	8.86
	PGD-4	84.22	8.86	86.58	5.62	74.53	17.49	82.45	9.33	29.55	31.7	74.43	10.37
	CosPGD-4	84.26	8.03	86.54	5.24	74.66	17.27	82.6	9.51	30.5	29.28	73.78	11.24
	VAFa-20	50.83	27.17	69.36	17.54	53.71	22.46	55.54	23.19	54.22	24.92	50.69	26.11
UMamba-E	FGSM-4	84.28	7.03	87.74	3.43	74.41	17.51	83.5	8.09	85.73	8.73	54.11	19.96
	PGD-4	85.13	6.02	89.17	3.39	75.56	17.04	83.65	8.09	87.36	6.35	28.09	29.77
	CosPGD-4	85.24	5.88	88.91	3.09	75.54	17.16	83.72	8.2	87.39	6.67	27.24	30.24
	VAFa-20	54.27	26.67	75.58	15.64	57.17	22.19	59.84	22.92	61.11	24.42	50.47	25.7

Table 9: Performance of models against transfer-based *black box* attacks on ACDC dataset. For pixel-based attacks results are reported for $\epsilon = \frac{4}{255}$ indicated by attack names followed by the suffixes -4 , respectively. Regarding frequency-based attack VAFa, the results are reported with a constraint on q_{\max} set to 20, denoted as VAFa-20. DSC score (*lower is better*) is reported on the generated adversarial examples.

Surrogate	Attack	UNet		SegResNet		UNETR		SwinUNETR		UMamba-B		UMamba-E	
		DSC↓	HD95↑	DSC↓	HD95↑	DSC↓	HD95↑	DSC↓	HD95↑	DSC↓	HD95↑	DSC↓	HD95↑
	Clean	75.72	9.15	80.84	8.14	72.53	15.08	78.07	10.01	78.37	8.12	77.06	11.11
	GN	75.40	10.31	80.34	8.44	72.33	14.45	77.44	9.73	77.69	9.44	75.34	21.80
UNet	FGSM-8	49.49	48.23	77.98	9.49	70.51	15.99	74.97	12.26	74.64	10.03	71.84	25.95
	PGD-8	32.06	89.45	79.78	8.73	72.02	15.28	76.89	10.69	76.92	9.02	74.74	13.86
	CosPGD-8	32.51	75.89	79.78	8.71	71.99	14.94	76.87	11.02	76.83	10.36	74.79	16.50
	VAFa-30	19.49	86.75	34.39	53.31	45.49	34.68	41.48	37.00	29.00	57.25	19.38	71.95
SegResNet	FGSM-8	71.70	12.01	59.97	37.36	69.93	15.34	72.48	11.81	68.73	14.77	67.95	22.74
	PGD-8	73.34	13.94	20.11	100.13	70.74	15.15	74.95	12.29	70.79	14.25	70.08	21.67
	CosPGD-8	73.29	13.76	19.68	96.74	70.75	15.12	75.04	11.75	70.50	14.16	69.79	21.31
	VAFa-30	36.43	44.43	22.00	72.16	50.16	28.19	45.54	36.83	28.39	55.87	19.53	69.45
UNETR	FGSM-8	70.89	12.07	76.13	10.51	50.98	44.86	71.48	12.97	72.47	10.35	71.21	15.05
	PGD-8	72.24	13.49	78.46	9.57	48.01	53.78	74.64	12.62	74.62	10.29	72.73	15.29
	CosPGD-8	72.31	13.61	78.73	9.29	47.46	51.14	74.83	13.44	74.78	9.80	72.81	15.43
	VAFa-30	40.27	35.24	42.55	34.84	26.68	58.83	41.90	39.54	36.16	43.97	31.47	45.45
SwinUNETR	FGSM-8	71.47	12.58	75.09	10.86	68.94	15.74	58.80	40.84	71.88	11.46	70.15	19.12
	PGD-8	72.28	13.68	77.92	9.61	70.17	17.17	54.09	64.43	74.62	11.56	72.19	20.70
	CosPGD-8	72.40	14.59	77.87	9.71	70.20	18.13	52.93	58.46	74.72	12.03	72.19	21.12
	VAFa-30	29.22	54.11	30.30	44.20	38.69	38.22	24.30	62.38	25.69	49.59	21.96	56.46
UMamba-B	FGSM-8	71.39	14.14	71.96	13.29	70.13	15.97	72.63	12.73	58.63	35.45	65.75	23.13
	PGD-8	73.27	12.02	76.11	12.59	71.06	15.61	75.59	12.31	30.08	98.04	67.72	23.63
	CosPGD-8	73.30	12.92	76.41	12.78	71.11	14.97	75.74	11.72	30.96	82.75	68.26	25.44
	VAFa-30	35.18	42.78	30.45	49.72	46.93	34.42	42.89	38.19	16.65	79.04	17.01	73.73
UMamba-E	FGSM-8	72.59	12.33	75.69	11.32	70.49	16.27	74.48	11.02	71.36	14.58	53.59	45.54
	PGD-8	74.39	13.66	79.09	9.55	71.69	15.04	76.91	11.23	75.58	10.74	29.51	104.51
	CosPGD-8	74.41	13.73	79.14	9.94	71.75	15.38	76.95	11.24	75.83	11.52	31.10	79.69
	VAFa-30	44.08	36.78	42.47	36.74	53.61	25.57	54.41	25.99	32.90	47.13	16.45	91.35

Table 10: Performance of models against transfer-based *black box* attacks on BTCV dataset. For pixel-based attacks results are reported for $\epsilon = \frac{8}{255}$ indicated by attack names followed by the suffixes -8, respectively. Regarding frequency-based attack VAFa, the results are reported with a constraint on q_{\max} set to 30, denoted as VAFa-30. DSC score (*lower is better*) is reported on the generated adversarial examples.

Surrogate	Attack	UNet		SegResNet		UNETR		SwinUNETR		UMamba-B		UMamba-E	
		DSC↓	HD95↑	DSC↓	HD95↑	DSC↓	HD95↑	DSC↓	HD95↑	DSC↓	HD95↑	DSC↓	HD95↑
	Clean	76.79	19.72	80.89	13.30	71.35	27.73	79.33	25.79	81.08	15.51	78.05	18.31
	GN	76.13	21.97	77.59	18.16	71.13	34.37	78.95	29.09	79.33	16.78	76.27	18.16
UNet	FGSM-8	46.85	60.19	71.90	18.50	68.90	35.00	74.99	31.74	72.55	22.68	70.24	24.43
	PGD-8	29.14	90.85	76.35	15.56	70.19	32.92	77.73	28.77	77.22	19.29	74.47	20.15
	CosPGD-8	30.80	77.47	76.44	15.66	70.24	33.87	77.86	28.52	77.43	18.27	74.58	20.25
	VAFa-30	20.92	88.19	26.62	66.39	38.36	63.57	38.75	57.28	22.36	71.25	18.89	75.11
SegResNet	FGSM-8	70.50	23.59	50.73	49.07	68.71	34.66	74.29	27.96	64.91	29.14	63.94	26.72
	PGD-8	73.76	22.77	17.42	106.73	69.90	32.58	76.90	28.83	70.87	23.57	69.81	24.80
	CosPGD-8	74.07	24.07	18.88	102.25	69.93	32.26	77.00	29.17	71.59	23.13	70.36	23.56
	VAFa-30	38.47	51.36	17.68	84.91	43.33	54.59	45.00	47.85	22.43	63.84	19.75	64.63
UNETR	FGSM-8	70.38	23.55	71.68	16.66	48.48	58.85	71.54	31.48	71.70	25.19	69.28	21.42
	PGD-8	72.57	22.99	74.85	17.19	44.83	76.08	75.28	30.96	74.82	18.84	70.82	23.81
	CosPGD-8	72.67	22.73	75.11	17.05	44.64	74.34	75.46	30.61	74.82	18.47	71.00	23.05
	VAFa-30	39.68	48.60	32.63	56.05	22.34	88.08	38.11	54.49	29.60	54.23	26.77	58.62
SwinUNETR	FGSM-8	69.99	24.44	69.39	18.48	66.81	35.05	53.46	71.03	70.21	23.45	68.12	23.85
	PGD-8	72.67	24.14	73.19	18.20	68.77	38.35	46.95	88.88	74.39	23.43	71.40	24.23
	CosPGD-8	72.88	23.67	73.56	18.34	68.85	38.09	46.79	82.92	74.59	22.30	71.67	23.91
	VAFa-30	30.47	60.63	27.51	60.51	33.10	64.36	25.43	76.41	24.11	65.63	22.06	65.39
UMamba-B	FGSM-8	70.60	24.91	65.06	23.98	68.69	35.94	74.25	31.40	51.36	53.89	62.19	30.01
	PGD-8	73.49	22.17	69.75	21.84	69.93	32.71	76.89	28.43	18.20	111.79	65.72	28.54
	CosPGD-8	73.46	22.99	70.35	20.94	69.94	33.08	76.92	28.69	18.99	101.89	66.36	30.04
	VAFa-30	38.49	55.47	24.20	65.44	43.80	58.37	44.61	52.18	14.99	92.09	18.46	69.64
UMamba-E	FGSM-8	70.93	23.48	68.27	20.87	68.69	35.07	74.85	29.52	65.66	30.35	48.81	52.13
	PGD-8	74.20	21.71	73.82	17.58	70.25	32.12	77.55	28.89	71.18	23.11	23.59	96.84
	CosPGD-8	74.41	21.16	74.15	17.06	70.30	32.56	77.65	28.78	71.86	22.90	24.99	82.01
	VAFa-30	39.41	53.15	27.39	61.14	43.32	58.63	46.53	50.97	23.31	72.51	13.88	92.91

Table 11: Performance of models against transfer-based *black box* attacks on Abdomen-CT dataset. For pixel-based attacks results are reported for $\epsilon = \frac{8}{255}$ indicated by attack names followed by the suffixes -8, respectively. Regarding frequency-based attack VAFa, the results are reported with a constraint on q_{\max} set to 30, denoted as VAFa-30. DSC score (*lower is better*) is reported on the generated adversarial examples.

Surrogate	Attack	UNet		SegResNet		UNETR		SwinUNETR		UMamba-B		UMamba-E	
		DSC↓	HD95↑	DSC↓	HD95↑	DSC↓	HD95↑	DSC↓	HD95↑	DSC↓	HD95↑	DSC↓	HD95↑
	Clean	73.91	11.36	74.73	11.08	72.36	14.61	71.61	22.07	73.50	10.89	72.19	13.29
	GN	72.11	12.97	73.26	10.08	71.28	14.51	69.61	23.65	72.12	13.96	66.58	13.45
UNet	FGSM-8	43.78	37.79	59.11	18.23	66.49	17.23	58.76	30.61	59.26	18.63	57.47	19.08
	PGD-8	34.07	78.61	68.24	13.80	69.87	17.54	64.99	27.33	67.38	14.62	65.55	17.80
	CosPGD-8	34.22	78.62	69.48	12.92	70.02	16.83	66.11	26.00	68.58	13.11	66.21	16.10
	VAFa-30	44.30	42.19	68.81	14.80	63.10	18.37	65.10	22.05	64.99	17.93	60.37	21.85
SegResNet	FGSM-8	60.62	21.43	47.70	32.24	67.51	17.17	57.01	30.20	53.92	27.12	55.13	21.08
	PGD-8	61.85	20.89	33.02	81.17	68.59	17.13	58.63	29.07	51.21	31.48	54.53	25.55
	CosPGD-8	61.99	19.89	33.41	81.28	68.81	16.63	58.74	29.19	50.25	32.25	54.15	23.28
	VAFa-30	69.07	17.77	47.55	33.08	66.24	17.71	65.55	21.85	65.23	17.79	62.22	23.54
UNETR	FGSM-8	58.16	19.27	59.01	15.60	44.89	35.08	54.29	31.27	57.88	17.11	56.95	19.62
	PGD-8	58.33	20.35	61.02	16.89	34.93	74.58	55.55	32.75	60.38	19.40	58.98	17.85
	CosPGD-8	59.02	21.18	61.97	17.29	34.89	73.84	56.13	32.29	61.55	19.64	59.95	20.11
	VAFa-30	64.73	19.36	69.68	13.81	48.01	33.82	57.85	27.53	65.38	19.19	58.59	21.28
SwinUNETR	FGSM-8	57.96	21.82	55.59	18.97	64.66	19.39	43.82	52.95	54.54	24.71	53.39	21.48
	PGD-8	55.25	25.87	56.09	20.16	66.29	19.83	34.12	78.85	55.14	23.72	54.18	23.60
	CosPGD-8	55.83	23.88	56.61	21.35	66.53	19.43	34.21	77.62	55.37	25.18	54.70	23.08
	VAFa-30	65.58	19.76	68.38	15.46	61.97	20.25	44.44	42.14	65.93	16.53	58.56	20.68
UMamba-B	FGSM-8	60.34	18.63	55.50	18.78	67.23	16.73	56.29	33.02	50.16	30.12	54.51	19.86
	PGD-8	61.83	19.34	49.65	39.99	69.07	16.88	58.12	31.30	34.31	78.39	51.03	30.70
	CosPGD-8	61.87	20.34	48.57	40.81	69.12	17.61	59.05	31.02	34.41	78.44	51.39	31.16
	VAFa-30	66.61	20.86	64.99	16.32	64.11	18.50	64.53	21.53	49.27	35.99	58.52	22.13
UMamba-E	FGSM-8	62.64	16.67	59.29	16.55	68.43	17.10	60.34	29.29	57.49	22.28	47.15	31.65
	PGD-8	69.30	14.95	68.77	12.22	70.59	15.53	66.92	25.14	66.75	16.73	34.29	78.25
	CosPGD-8	69.55	13.86	69.49	12.88	70.67	15.07	67.34	26.04	67.43	16.99	34.37	77.85
	VAFa-30	68.09	20.51	69.84	13.90	64.26	19.12	65.86	24.17	66.03	20.12	44.81	36.84

Table 12: Performance of models against transfer-based *black box* attacks on HeCtor dataset. For pixel-based attacks results are reported for $\epsilon = \frac{8}{255}$ indicated by attack names followed by the suffixes -8, respectively. Regarding frequency-based attack VAFa, the results are reported with a constraint on q_{\max} set to 30, denoted as VAFa-30. DSC score (*lower is better*) is reported on the generated adversarial examples.

Surrogate	Attack	UNet		SegResNet		UNETR		SwinUNETR		UMamba-B		UMamba-E	
		DSC↓	HD95↑	DSC↓	HD95↑	DSC↓	HD95↑	DSC↓	HD95↑	DSC↓	HD95↑	DSC↓	HD95↑
	Clean GN	85.52	5.75	89.65	2.56	76.37	16.31	84.19	7.93	88.22	6.01	80.91	8.48
		85.01	5.67	89.26	2.89	74.88	18.49	83.06	10.69	86.95	6.68	78.11	11.67
UNet	FGSM-8	55.55	21.99	86.65	4.55	73.32	18.87	81.12	11.22	84.58	11.19	74.96	13.42
	PGD-8	21.42	39.14	88.05	5.21	74.67	18.96	82.57	10.59	86.32	10.08	77.82	10.82
	CosPGD-8	22.62	36.84	88.18	5.12	74.36	18.73	82.92	10.12	86.50	9.92	77.33	11.97
	VAFa-30	49.85	27.44	74.15	18.17	56.09	21.77	58.72	22.95	60.27	24.46	53.68	25.98
SegResNet	FGSM-8	83.63	6.32	66.58	11.88	73.03	19.72	80.41	12.75	81.15	19.95	74.57	14.46
	PGD-8	84.38	6.34	20.42	37.34	74.59	17.62	82.27	9.84	85.72	10.48	76.39	11.34
	CosPGD-8	84.54	6.08	22.33	38.61	74.79	18.05	82.44	9.58	85.69	9.58	76.41	11.32
	VAFa-30	51.83	27.22	54.47	23.38	54.96	21.60	57.00	24.20	59.24	24.27	53.12	25.38
UNETR	FGSM-8	80.15	12.78	83.33	6.48	33.16	29.77	75.79	16.74	77.48	25.93	72.88	14.93
	PGD-8	83.25	13.69	85.54	7.19	22.31	35.44	80.12	15.19	80.67	22.48	68.37	16.98
	CosPGD-8	82.98	13.48	86.08	7.09	23.08	34.80	80.12	15.41	81.37	21.11	70.52	17.51
	VAFa-30	52.67	26.66	74.18	15.78	49.39	22.63	55.90	24.47	58.27	24.85	52.16	25.09
SwinUNETR	FGSM-8	83.11	7.61	81.34	5.11	71.91	18.15	56.11	21.83	80.69	15.61	74.72	11.74
	PGD-8	84.04	7.49	84.37	6.75	71.73	19.22	21.69	36.99	82.42	15.23	72.15	12.77
	CosPGD-8	83.92	7.75	84.38	7.25	71.91	20.24	22.50	36.20	83.34	19.98	70.49	13.23
	VAFa-30	51.50	26.94	70.18	17.16	53.50	23.25	48.44	25.57	57.68	25.01	52.52	25.27
UMamba-B	FGSM-8	81.55	14.53	83.27	5.11	71.83	19.99	79.61	13.74	72.55	21.19	71.54	14.86
	PGD-8	82.82	12.81	82.49	6.18	72.14	19.13	79.95	12.33	24.95	34.66	69.66	15.29
	CosPGD-8	82.58	10.26	82.69	7.37	72.50	18.78	80.14	11.97	25.54	31.32	68.93	14.86
	VAFa-30	51.46	27.35	71.36	17.79	54.18	22.82	57.14	13.39	53.38	25.22	51.83	26.27
UMamba-E	FGSM-8	82.44	13.41	84.96	4.75	71.23	20.59	81.82	12.16	81.97	15.77	51.65	24.22
	PGD-8	84.66	6.11	87.71	3.43	74.51	18.16	82.95	9.17	86.12	7.46	25.01	32.43
	CosPGD-8	84.79	6.32	87.31	3.84	74.86	17.58	83.01	9.52	86.19	7.14	24.44	31.55
	VAFa-30	55.01	27.08	75.57	15.77	57.40	20.80	60.22	23.85	61.26	24.54	51.61	25.72

Table 13: Performance of models against transfer-based *black box* attacks on ACDC dataset. For pixel-based attacks results are reported for $\epsilon = \frac{8}{255}$ indicated by attack names followed by the suffixes -8, respectively. Regarding frequency-based attack VAFa, the results are reported with a constraint on q_{\max} set to 30, denoted as VAFa-30. DSC score (*lower is better*) is reported on the generated adversarial examples.

Surrogate	Attack	BTCV		ACDC		Hecktor		Abdomen-CT	
		DSC↓	IoU↓	DSC↓	IoU↓	DSC↓	IoU↓	DSC↓	IoU↓
UNet	FGSM-8	72.56	60.84	61.74	48.09	36.41	24.66	76.73	65.07
	PGD-8	73.23	61.39	60.44	46.54	36.15	24.55	77.15	65.53
	CosPGD-8	73.34	61.51	60.50	46.68	36.32	24.59	77.05	65.44
	VAFa-30	66.26	53.80	47.01	35.51	36.77	24.70	69.82	56.99
SegResNet	FGSM-8	73.16	61.34	63.15	49.86	36.64	24.73	76.82	65.21
	PGD-8	72.95	61.24	61.38	47.64	34.98	23.57	76.84	85.27
	CosPGD-8	73.05	61.31	61.99	48.35	34.76	23.38	76.92	65.32
	VAFa-30	66.28	53.76	45.13	33.64	36.27	24.39	71.57	58.92
UNETR	FGSM-8	71.59	59.82	61.18	47.65	37.52	25.49	75.49	63.66
	PGD-8	72.15	60.33	58.93	45.80	38.19	26.08	76.15	64.44
	CosPGD-8	72.34	60.46	59.74	46.55	38.32	26.37	76.16	64.43
	VAFa-30	65.31	52.77	45.16	33.43	40.00	27.24	68.35	55.07
SwinUNETR	FGSM-8	73.05	61.19	62.72	48.68	35.94	24.20	76.54	64.91
	PGD-8	73.06	61.23	61.59	47.82	36.35	24.81	76.67	64.99
	CosPGD-8	73.04	61.26	61.32	47.65	36.21	24.62	76.82	65.22
	VAFa-30	65.23	52.59	43.32	31.76	38.61	26.12	68.03	54.81
UMamba-B	FGSM-8	72.93	61.12	62.85	49.62	36.86	25.05	76.83	65.23
	PGD-8	72.94	61.16	60.10	46.45	35.56	24.09	77.01	65.38
	CosPGD-8	73.17	61.34	60.91	46.99	36.37	24.64	77.12	65.54
	VAFa-30	65.47	53.15	44.51	32.98	37.54	25.41	71.61	58.82
UMamba-E	FGSM-8	73.03	61.19	63.56	50.06	36.95	25.04	77.01	65.38
	PGD-8	73.04	61.28	60.56	46.78	35.72	24.14	77.15	65.53
	CosPGD-8	73.24	61.42	61.15	47.62	35.67	24.17	77.02	65.43
	VAFa-30	67.43	55.23	45.47	34.04	36.55	24.63	71.47	58.75

Table 14: Evaluating SAM-Med3D on adversarial examples crafted on surrogate models trained on BTCV, ACDC, Hecktor, and Abdomen-CT datasets.